aerospace

MDPI

Article

Combined Sizing and Aircraft Evaluation of an Electrically Assisted Propulsion System

Philipp Maas *, Christopher Warsch, Arne Seitz and Mirko Hornung

Bauhaus Luftfahrt e.V., Willy-Messerschmitt-Str. 1, 82024 Taufkirchen, Germany; christopher.warsch@web.de (C.W.); arne.seitz@bauhaus-luftfahrt.net (A.S.); mirko.hornung@bauhaus-luftfahrt.net (M.H.)

* Correspondence: philipp.maas@bauhaus-luftfahrt.net

Abstract

The design of hybrid electric propulsion (HEP) systems involves multiple sizing requirements and operating conditions that affect aircraft performance. Assessing their overall potential requires the coupled consideration of hybridization, battery technology, mission utilization and operational constraints. Therefore, an integrated methodology combining HEP sizing with simplified aircraft design and performance methods is presented. A parallel HEP concept with an electrically assisted compressor is investigated for a 50 PAX regional aircraft and a 19 PAX helicopter, considering an Entry-Into-Service (EIS) in Y2035+. To enable operation without electrical assistance, gas turbine oversizing is applied. This comes with mass and efficiency penalties but significantly expands the operational hybridization range. At a battery system specific energy of 500 Wh/kg, the regional aircraft achieves a 1% block fuel reduction on the design mission (400 nmi), compared with a 22% reduction on the shorter typical mission (150 nmi) through increased battery utilization. For the helicopter, block fuel increases by 11% on the design mission, but decreases by 10% on the typical mission. The results demonstrate that aircraft utilization is a key factor for the sizing and assessment of parallel HEP systems.

Keywords: hybrid electric aircraft; hybrid electric propulsion; parallel hybrid propulsion; cycle-integrated parallel hybrid; propulsion system design; aircraft design; aircraft performance; compressor electric drive; regional aircraft; helicopter

1. Introduction

Many advanced propulsion systems for aeronautical applications excel with respect to overall efficiency, but show significant drawbacks in terms of size, weight and operational implications. HEP systems are no exception to this, as the true potential of these technologies only becomes evident at the aircraft level.

For more than a decade, significant progress has been made on the fundamental methodology and sizing strategies for hybrid electric propulsion and aircraft systems [1–6]. The underlying battery technology, particularly the specific energy, has been identified as the most critical factor for the success of hybrid electric aircraft. Recent research shows that battery specific energy values of up to 600 Wh/kg could be achieved by 2035–2040, e.g., by utilizing advanced lithium-sulfur chemistries [7,8]. This makes the application for regional turboprop aircraft especially attractive, as for these battery technologies tangible fuel burn improvements are expected for design ranges of up to 600 nmi [9–11].

Academic Editor: Patrick J. Norman

Received: 2 September 2026
Revised: 23 October 2026
Accepted: 26 October 2026
Published: 1 November 2026

Copyright: © 2026 by the authors. Licensee MDPI, Basel, Switzerland. This article is an open access article distributed under the terms and conditions of the Creative Commons Attribution (CC BY) license.

Various HEP architectures can be examined, with the most common ones being either serial hybrid or parallel hybrid configurations [12,13]. Serial hybrids primarily aim at improving system-level efficiency by enhancing the propulsion–airframe integration, e.g., through Distributed Electric Propulsion (DEP) or Boundary Layer Ingestion (BLI). Parallel hybrids, on the other hand, target improved propulsion system efficiency by utilizing the more efficient electric power train through electrical assistance.

Numerous integrated parallel hybrid configurations have been investigated at the propulsion system level. The most common ones are the Cycle-Integrated Parallel Hybrid (CIPH), the Mechanically Integrated Parallel Hybrid (MIPH) or a combination of both systems (see Figure 1). In a CIPH system, the electrical energy is directly fed to the engine core, e.g., via partially driving the compressor, aiming at improving the operational flexibility, part-load efficiency or core size of the engine [14,15]. A MIPH system injects the electrical power directly to the propulsor (e.g., to the output shaft), hence minimizing the transmission losses by mechanical connection [2,12]. Combining both systems increases overall complexity, but also enhances redundancy and operational flexibility, e.g., by adapting the power addition to the low- and high-pressure spool [16–19].

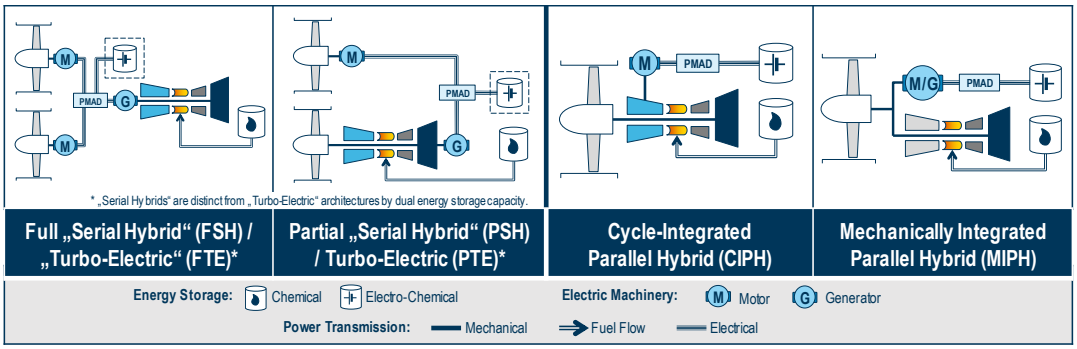


Figure 1. Overview of selected hybrid electric propulsion system architectures (from [12]).

However, the amount of power that can be added or extracted from the gas turbine is also restricted by mechanical limitations (e.g., spool speeds), thermodynamic bounds (e.g., maximum temperatures) or aerodynamic constraints within the turbo components (e.g., compressor surge) [12,15–17,20,21]. This not only limits the maximum achievable hybridization degree, but also impacts the operability of the propulsion system in case of electric system failure [12,15]. While previous studies captured both effects in detail at the propulsion system level, they also have a large impact on mission fuel burn and thus need to be addressed at the overall aircraft level as well.

Numerous parallel hybrid electric aircraft-integrated studies have been performed over the last years, differing in terms of aircraft class, battery technology, hybridization approaches or propulsion system architecture. The first studies focused on the impact of different battery technologies and hybridization degrees on overall design mission fuel burn [11,22,23]. Other studies concentrated on the HEP scalability by analyzing different design ranges [9,12]. As regional aircraft are mostly operated far below their design range, later research included the performance evaluation of a typical mission [24–26] or additional off-design missions [27,28].

Not only fixed-wing aircraft, but also hybrid electric rotorcraft have been investigated over the past years. Initial studies examined the overall potential of parallel-hybrid propulsion systems for a mid-sized helicopter application [14,29]. The most universal approach was performed in [30], analyzing different hybridization degrees and its impact on design mission performance and payload–range capacity. In addition, more detailed studies on hybrid electric rotorcraft have been performed, focusing on specific aspects

such as pollutant emissions, energy management strategies or recuperated engine cycles [31–33].

Despite the increasing number of parallel hybrid electric studies performed at the aircraft level, at least one out of four common limitations can be identified:

1. The HEP components are sized only for one or a few specific hybridization levels; hence, the impact of different hybridization degrees on the overall aircraft sizing and mission performance is not well understood.
2. The key technology assumption, namely the battery specific energy, is held constant, preventing an adequate interpretation of the overall results.
3. Only the design mission is considered, disregarding the significant advantages that parallel HEP systems offer when fully utilizing the available battery capacity on shorter, typically flown off-design missions.
4. The operational constraints of the propulsion system and non-normal cases such as electrical system failure are not considered, neglecting the impact on propulsion system sizing and performance.

Actually, several recent studies have significantly advanced the understanding of the off-design performance behavior of parallel hybrid electric aircraft [34–38]. They describe in detail the impact of different payload–range mission requirements on the overall performance, fuel burn and battery utilization. Nevertheless, these investigations do not fully consider the operational implications at the propulsion system level and are usually performed for one specific battery technology only.

On the other hand, the impact of failure cases on the overall aircraft performance has been considered in [39,40]; however, these studies do not include sensitivities with regard to different off-design missions or different hybridization levels.

To further support the identified research gap, Table 1 provides an overview of previous aircraft studies and compares them based on the four limitations mentioned above.

Table 1. Comparison of relevant literature on parallel hybrid electric aircraft studies with respect to the four methodological aspects identified.

References	Variation in Hybridization Degree	Variation in Battery Specific Energy	Consideration of Typical/Off-Design Mission	Consideration of Propulsion System Constraints
[1,23]	●	o	x	x
[9,11,22]	●	●	x	x
[24,36,37]	o	x	●	x
[38]	●	x	●	x
[5,25,26]	●	o	●	x
[34,35]	o	x	●	o
[27]	●	o	x	o
[14]	●	x	x	●
[12]	o	●	x	●
[39]	o	o	x	●
Current study	●	●	●	●

● fully covered; o partially covered; x not covered.

Traditionally, complex hybrid electric aircraft-integrated studies are performed using sophisticated aircraft design environments such as SUAVE [41], BLADE [42] or Initiator [43]. They provide advanced aircraft sizing and mission analysis capabilities and are well suited for the conceptual design of various aircraft configurations. However, especially for HEP applications, propulsion system sizing requires multiple sizing-relevant operating conditions, while the operational behavior varies with the selected

hybridization degree. Hence, conventional aircraft design approaches require repeated iterations between propulsion system and aircraft design, typically depending on the laborious creation of engine design and performance datasets. In order to efficiently capture these coupled interactions, a rapid aircraft evaluation methodology enabling the extensive parametric investigation of advanced propulsion systems is required [44].

Compared with existing integrated propulsion system and aircraft design and performance approaches (e.g., [45]), the presented methodology specifically focuses on the sizing and operational implications of parallel HEP systems. It enables the investigation of different hybridization levels and their impact on both component sizing and aircraft performance, while accounting for the allowable hybridization range and electric system failure. Furthermore, the methodology considers both design and off-design missions as a key enabler to assess the battery utilization and the overall benefits of parallel HEP systems. Additionally, it allows for extensive parametric studies across different battery technologies, design requirements or aircraft applications.

The methodology is demonstrated using an innovative CIPH propulsion concept with electrical assistance of the compressor section, as part of the German national-funded project HybVer [46]. It is applied to two aircraft categories: a 50 PAX regional aircraft and a 19 PAX medium-sized helicopter. Parametric studies for different hybridization degrees and battery specific energy assumptions are performed for both applications, assessing the resulting effects on propulsion system sizing and aircraft performance. The resulting fuel consumption is then compared with a non-hybrid conventional aircraft with the same technology assumptions and EIS. In addition, the scalability of the proposed propulsion concept is investigated for the regional application by design range sensitivity studies.

The paper is organized as follows: Section 2 provides an overview of the propulsion system concept, the aircraft applications and technology assumptions. Section 3 explains the methodology in detail, with an emphasis on the hybrid electric propulsion system and its integration in the overall framework. Section 4 presents the propulsion system and aircraft performance results for both applications, evaluated for the design and typical mission. Finally, the results are discussed in Section 5, while the last section provides the main conclusions of this paper and inspirations for future work.

2. Application Cases

2.1. Propulsion System Concept with Compressor Electric Drive

The investigated HybVer propulsion system concept is based on a CIPH architecture employing a two-shaft turboshaft layout. The electrical power is directly injected into the compressor section, thus enabling a partial replacement of the turbine work while utilizing the higher efficiency of the electric drive train. The propulsion system comprises a counter-rotating compressor (CRC) section together with a radial high-pressure compressor, both mounted on the same shaft. Figure 2 displays a schematic representation of the hybrid electric propulsion system for the regional aircraft application.

Electrical energy is supplied by a battery system integrated into the aircraft based on the concepts shown in [26,47]. The electrical power is then routed through the power management and distribution (PMAD) system towards two electric machines. One directly assists the shaft of the core engine (Motor A), while the other electrically drives the outer rotors of the counter-rotating compressor (Motor B). Motor A is integrated upstream of the compressor section within the hub region, whereas Motor B is mounted on the outer casing of the counter-rotating compressor. Both motors utilize conventional mechanical bearings connected to the turbo machinery struts.

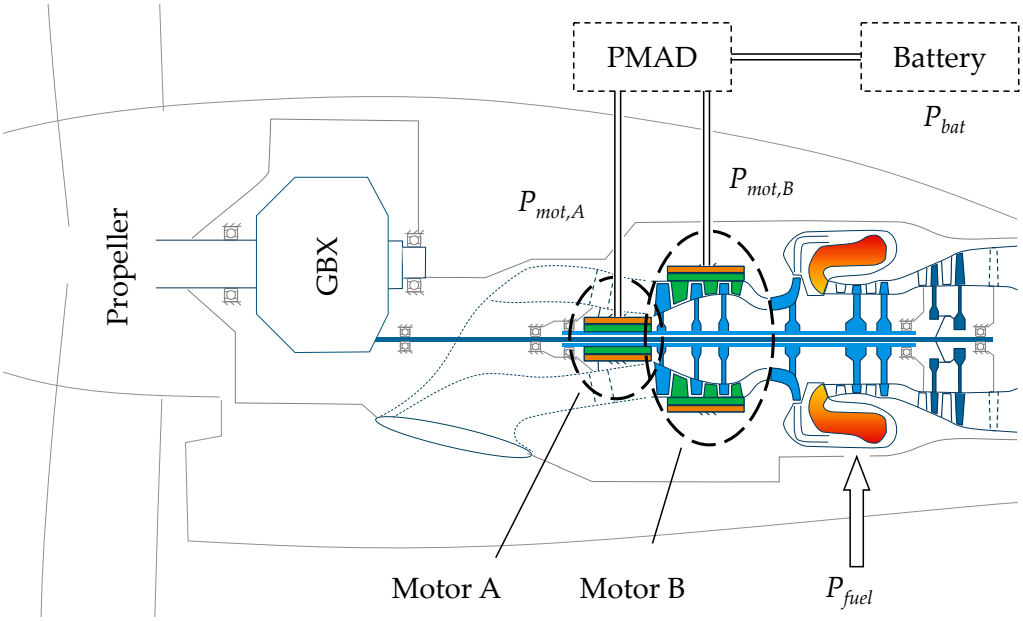


Figure 2. Concept sketch of the investigated cycle-integrated parallel hybrid electric propulsion concept, featuring electrical assistance to the core shaft (Motor A) and the outer rotors of the counter-rotating compressor (Motor B).

The use of two electric machines enables more flexible power distribution within the propulsion system and offers higher system redundancy. In case one electric machine fails, the available electrical energy in the battery system can be re-routed to the remaining operating machines. Additionally, Motor A can operate in generator mode and provide electrical power to Motor B in case the electrical supply is cut. This allows Motor B to ensure continuous operation of the outer CRC rotors, thus preventing an engine shutdown.

To achieve high electrical efficiencies, both electric motors use a Permanent Magnet Synchronous Machine (PMSM) topology utilizing a Halbach array rotor configuration to increase power density. On the stator side, Motor A uses a conventional winding arrangement, whereas Motor B uses a toroidal winding configuration to maximize axial compactness [48]. Each electric machine is individually designed to its specific torque and rotational speed requirements, considering the spatial constraints and maximum allowable circumferential rotor speeds [48,49]. Rotor cooling is achieved through an insulation layer between the compressor rotor disk and the permanent magnets as well as by airflow through the air gap [50]. For stator cooling, a Thermal Management System (TMS) employing a liquid cooling system in a helical coil configuration is used, providing a trade-off between cooling performance and pressure losses [50]. Furthermore, the aerodynamic design of the counter-rotating compressor is adapted to account for the unequal work split between the mechanically and electrically driven rotors [51]. This is necessary as the amount of electrical power that can be provided to the electrically driven compressor rotor section is limited by the maximum electric rotor tip speed [15].

For the design of the parallel hybrid electric propulsion concept, two important descriptors are introduced. First, the degree of power hybridization H_P defines the share of electrical supplied power $P_{sup,el}$ relative to the total supplied power $P_{sup,tot}$ [4]:

$$H_P = \frac{P_{sup,el}}{P_{sup,tot}} = \frac{P_{bat}}{P_{bat} + P_{fuel}}. \quad (1)$$

Here, P_{bat} is the electrical power supplied to the battery system to drive both electric power trains, while P_{fuel} is the thermal power of the fuel provided to the combustor.

During the design mission, the design degree of hybridization $H_{P,des}$ is set to size both the battery system and the gas turbine components. In off-design operation, the off-design degree of hybridization $H_{P,od}$ is used to control the level of electrical power supplied to the engine.

The second metric is the electric power split $S_{P,elec}$, which is introduced to distribute the electrical power between both electric drive trains [16]. It is used to control the operability of the counter-rotating compressor and is defined as:

$$S_{P,elec} = \frac{P_{mot,A}}{P_{mot,tot}} = \frac{P_{mot,A}}{P_{mot,A}+P_{mot,B}}, \quad (2)$$

where $P_{mot,A}$ is the electric motor shaft power supplied to the HP shaft, $P_{mot,B}$ the electric motor shaft power provided to the counter-rotating compressor, with $P_{mot,tot}$ being the total output shaft power from both electric motors.

2.2. Aircraft Application Cases

The proposed hybrid electric propulsion system is investigated for two different aircraft categories: a fixed-wing regional aircraft and a super-medium civil transport helicopter. This enables an assessment of whether this type of propulsion concept can also be applied to other market segments and operating scenarios.

For the regional aircraft, an ATR42-class aircraft is selected as the 50 PAX state-of-the-art reference (REF) aircraft, while an AW189K-class helicopter is chosen as the 19 PAX reference for the helicopter application. Based on these reference aircraft, the non-hybrid baseline aircraft configurations (BAS) with an EIS in Y2035+ are derived by applying a projected technology level together with the HybVer project-specific Top Level Aircraft Requirements (TLARs). Subsequently, the hybrid electric aircraft (HYB) are obtained by integrating the HEP system with an electrically assisted compressor, employing the same technology level and TLARs as for the baseline cases. An overview of the workflow used to derive the HybVer aircraft applications is depicted in Figure 3:

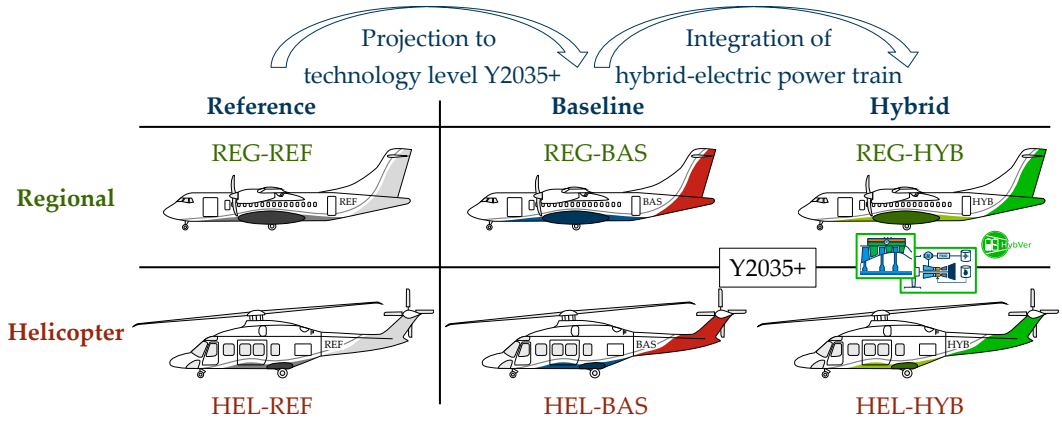


Figure 3. Concept derivation of the Y2035+ HybVer regional aircraft (REG) and helicopter (HEL) configurations.

For both regional and helicopter application cases, the selected TLARs with an EIS in Y2035+ are summarized in Table 2. They are applied to each baseline and hybrid aircraft application case. Typical number of passengers, cruise altitudes and speeds for both types of vehicles were assumed. For the regional aircraft, the cruise conditions are derived from the IMOTHEP project [26]. The design range selected for the Y2035+ helicopter applications remains comparable with the reference case, while the typical range was assumed and cross-checked against a limited number of publicly available flight tracking records. The ranges of the Y2035+ regional applications are adjusted based on existing operational

flight data [52]. Considering only flight movements of the ATR42 aircraft, the design mission range was selected to cover >90% of all flights, whereas the typical mission range was based on the most frequently observed flight range. Aircraft performance is evaluated for both the design mission and the typically flown mission. To reflect appropriate contingencies and reserve fuel, an equivalent range of 250 nmi is added to the main mission fuel demand for the regional application, whereas for the helicopter application, an additional 30 min of reserve fuel is added in accordance with [53].

Table 2. Top-level aircraft requirements (TLARs) for the regional aircraft and helicopter applications, assuming an entry-into-service in Y2035+.

Parameter	Unit	Regional	Helicopter
EIS	-	2035+	
Design mission range	nmi	400	200
Typical mission range	nmi	150	100
Number of passengers	-	50	19
Design payload	kg	5000	1900
Cruise speed	m/s	129 [1]	75
Cruise altitude	ft	15,000	3000
Reserves	nmi/min	250 nmi	30 min

[1] Corresponds to flight Mach number of 0.4.

2.3. Technology Settings

The projected technology assumptions for the regional and helicopter Y2035+ configurations are displayed in Table 3. For both aircraft categories, technology improvements regarding aerodynamics, mass and propulsion are assumed compared with the reference aircraft.

Table 3. Technology assumptions for the regional aircraft and helicopter applications, assuming an entry-into-service in Y2035+.

Discipline	Regional	Helicopter
Aerodynamics	Increased wing aspect ratio from 11 to 14	Improvement of EFPA/A_{rot} from 0.014 to 0.010
Weights	Constant relative masses per MTOM	10% reduction of helicopter empty mass
Propulsive efficiency	Increase propeller efficiency from 85% to 87%	Constant helicopter main rotor efficiency

Aerodynamic improvements are assumed for both aircraft categories, with the regional aircraft benefiting from an increased wing aspect ratio [26] and the helicopter from a more streamlined helicopter fuselage, reducing the Equivalent Flat Plate Area (EFPA) [54]. The ratio of the masses for aircraft structures, systems and equipment (excluding the HEP components) to the Maximum Take-Off Mass (MTOM) is kept constant for the regional aircraft. For the helicopter application, a reduction of 10% is assumed to consider its higher lightweighting potential. For the Y2035+ baseline power plant systems, suitably advanced technology settings are adopted, leading to double-digit improvements in thermal efficiency. These account for higher core temperatures, advanced cooling technologies and better component efficiencies. In terms of propulsive efficiency, no significant improvements are assumed for the helicopter rotor efficiency, whereas a slight increase in propeller efficiency is considered for the regional application.

In addition to the evolutionary technology improvements, the technology assumptions for the hybrid electric power train components are summarized in Table 4. The most important technology parameter, the battery specific energy, is set as a study parameter to analyze its impact on overall aircraft performance. The remaining component assumptions are directly derived from literature.

Table 4. Hybrid electric power train component technology assumptions for the regional aircraft (REG) and helicopter (HEL) applications.

Parameter	Unit	REG	HEL	Remark
Battery specific energy (system level)	Wh/kg	400–600		Study parameter for subsequent aircraft studies.
Battery discharge efficiency	%	95		Source: [26]
Battery TMS specific mass	kg/kW	2.9		Based on heat loss to be dissipated. Source: [26]
Motor A gravimetric power density	kW/kg	16	7.6	Specifically designed for application. Source: [48]
Motor A design efficiency	%	96	97	Specifically designed for application. Source: [48]
Motor B gravimetric power density	kW/kg	5.5	4.9	Specifically designed for application. Source: [48]
Motor B design efficiency	%	97	95	Specifically designed for application. Source: [48]
PMAD gravimetric power density	kW/kg	5		Incl. converters, inverters, controllers, cables, PDU, considering redundant system layout. Source: [55]
PMAD efficiency	%	98		Source: [26]
El. motor and PMAD TMS specific mass	kg/kW	0.56		Based on heat loss to be dissipated. Source: [50]

3. Methodology

The overall purpose of the presented methodology is the preliminary parametric evaluation of aircraft performance under consideration of propulsion system behavior and key design parameters. For this, detailed propulsion system synthesis is combined with simplified aircraft sizing heuristics and analytical performance methods. Instead of treating propulsion system sizing and aircraft design separately, propulsion-integrated aircraft studies can be performed at an early stage, reducing the number of iterations between both disciplines compared with the conventional approach. Special emphasis is placed on the consideration of multiple sizing-relevant operating conditions, operational boundaries and abnormal operating scenarios. This becomes especially important for hybrid electric applications, where the operational performance and limitations at the propulsion system level are strongly coupled with the sizing and mission performance at the aircraft level.

In the following sections, the overall methodological approach is outlined in the beginning, followed by a detailed description of the relevant modules with special emphasis on the hybrid electric propulsion system modeling. Lastly, the presented methodology is evaluated and compared with existing reference applications at the aircraft level to support the validity of the results.

3.1. Overall Approach

In the following section, the overall structure and workflow of the methodology are described. Figure 4 depicts an overview of the implemented sizing logic and the involved modules. Two iterative workflows are shown: a sizing loop used to perform the aircraft and propulsion system sizing at design conditions and an operational loop used to evaluate off-design mission performance for fixed component geometries and masses.

For the sizing loop, the TLARs and technology assumptions summarized in Tables 2 and 3 serve as an input, together with the selected design degree of hybridization $H_{P,des}$ and an initial estimation for MTOM. First, the aircraft geometry and mass module is called, calculating the wing or rotor dimensions as well as the overall component masses (including the HEP system) and Operating Empty Mass (OEM). Subsequently, the aerodynamic module is called to determine the aircraft drag and the resulting propulsion system power requirements. Based on that, the propulsion system is evaluated, providing fuel and electrical energy consumption at the relevant flight conditions. The subsequent mission analysis at the aircraft level calculates the resulting design mission fuel and energy demand. Finally, the updated fuel and battery masses are added to the aircraft mass breakdown and the initial MTOM estimation is updated, restarting the sizing loop.

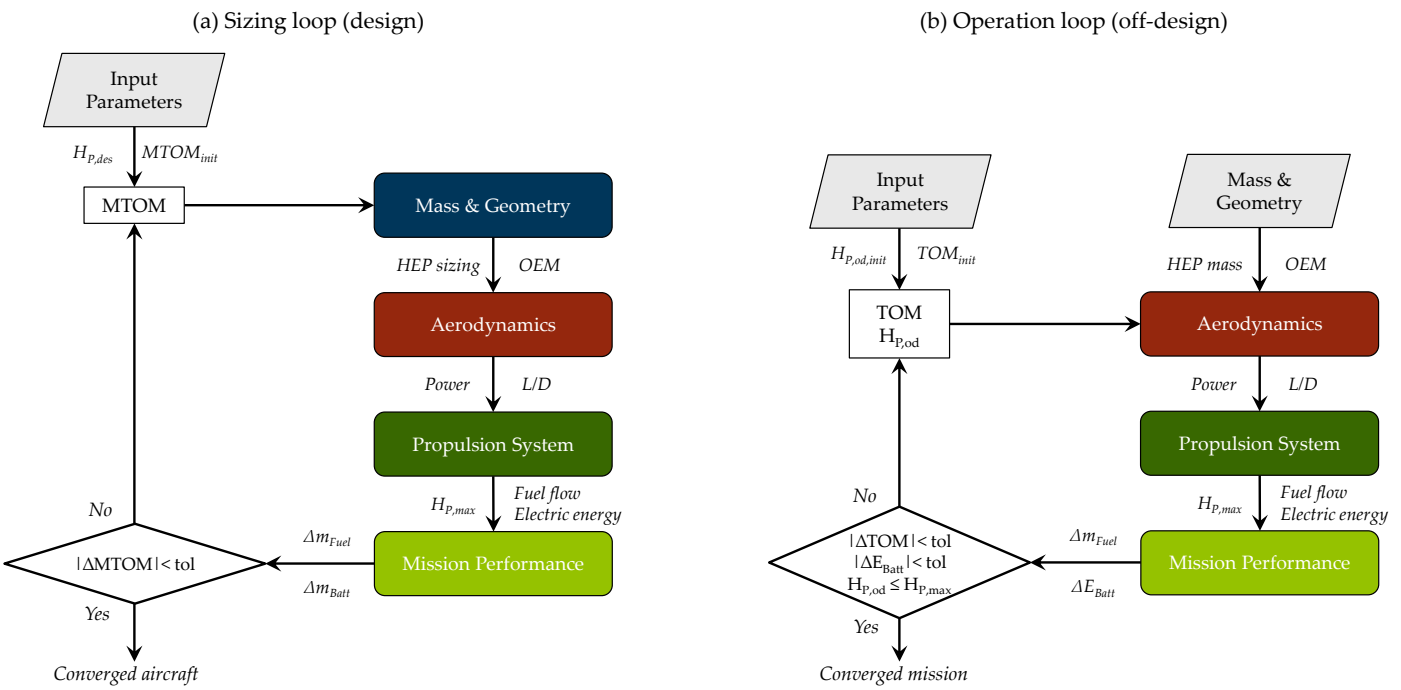


Figure 4. Implemented workflow for (**a**) the combined aircraft and HEP sizing (design) and (**b**) mission performance (off-design) evaluation.

During the iterative aircraft sizing, changes in mass (e.g., propulsion system, fuel or battery) directly affect the aircraft geometry, aerodynamic performance, overall power requirements and thus the resulting fuel and electrical energy consumption (snowball effect). Convergence is reached once the change in MTOM falls below a prescribed convergence criterion. After convergence of the sizing loop, the resulting design mission fuel mass and electrical energy consumption are saved, and the fully sized aircraft and propulsion system components, including the battery system, are provided to the operational loop.

The operational loop serves the evaluation of additional off-design missions with varying range or payload. For this, the component geometry and masses calculated from the sizing loop are fixed and the remaining aerodynamic, propulsion system and mission performance modules are executed sequentially (see Figure 4). Similar to the sizing loop, an initial estimation of the Take-Off Mass (TOM) is required for the mass iteration. In addition to the mass convergence, a hybridization iteration is performed to determine the achievable off-design degree of hybridization $H_{P,od}$. Since the battery system has already been sized in the sizing loop, the available battery capacity should be utilized as best as possible during the off-design mission. Therefore, the off-design hybridization degree is iteratively adjusted until convergence of the electrical energy consumption is achieved while remaining within the allowable operational limits of the propulsion system. The operational loop provides the resulting mission performance, including fuel and energy consumption, as well as the feasible off-design hybridization degree.

Despite investigating two completely different aircraft categories, the same integrated modular workflow is applied for both fixed-wing and rotary-wing applications, where the coupling between aircraft sizing, hybrid electric propulsion system sizing and battery utilization remains the same. However, discipline-specific methods are implemented for the aircraft geometry, mass, aerodynamics and mission evaluation due to the fundamentally different flight physics and operating characteristics.

For the regional application, the aircraft-level design and performance evaluation of the HybVer technology is conducted using the in-house developed Simplified Aircraft

Scaling (SAS) methodology as presented by Seitz [44]. This methodology offers a modular set of basic analytical and semi-empirical methods, enabling rapid evaluations of revolutionary propulsion concepts at the vehicular level, including first-order integration, sizing and performance cascade effects. The SAS framework is designed to easily allow the parametric mapping of advanced technology. This includes evolutionary improvements as well as technological step-changes in aerodynamics, structures, systems and propulsion. The foundation of SAS includes a library of basic aircraft design heuristics derived from a database of subsonic fixed-wing aircraft with entries into service between 1986 and 2013. Valid aircraft scaling results for a broad range of vehicles were demonstrated, with validation cases covering both turbofan- and turboprop-powered aircraft [44].

For the helicopter application, a new framework for rotorcraft sizing and performance analysis called the HelicOpter design and performance eValuation framEwoRk (HOVER) was developed. It serves for the assessment of conventional as well as future rotorcraft with advanced propulsion systems. The methodology is based on empirical data and handbook methods and integrates preliminary geometry and mass estimation, aerodynamic calculations, evaluation of power demand across different flight conditions, mission definition for representative helicopter operations and integrated propulsion system sizing to determine the overall mission fuel consumption. Rotorcraft scaling is achieved using semi-empirical sizing heuristics that include the fuselage drag, rotor disc loading or rotor solidity. One distinguishing feature is the direct coupling of the propulsion system performance synthesis model with the mission analysis module, enabling a mission point resolved analysis of the propulsion system requirements and direct evaluation of the engine parameters, e.g., during hover or transition to cruise. The HOVER framework was validated against a light utility helicopter and a super-medium transport helicopter application (see Section 3.7).

3.2. Geometry and Mass

3.2.1. Regional Aircraft

For the present study, a set of methods and scaling laws was selected from the libraries that is specially tailored to the needs of the HybVer technology case. Therefore, basic aircraft design and operational characteristics were specified as constants to reflect an ATR42-class aircraft throughout the study. This includes typical cruise conditions and wing scaling at a constant wing loading of 340 kg/m^2. The wing aspect ratio was set to 11, with wing sweep and taper ratio determined from heuristic functions of the assumed cruise Mach number. Fuselage dimensions (length and equivalent diameter) are also read from the library of aircraft design heuristics as a function of the design number of passengers. Propulsion system sizing is based on the cruise power requirement with adequate margin for low-speed operations. The propellers were assumed to be 6-bladed with a disc loading of 82 kW/m^2 and the corresponding efficiency at the typical cruise point.

For the overall aircraft mass modeling, OEM is divided into three main groups of mass items, namely structures, systems and equipment, and propulsion, each of which is mapped as relative shares of aircraft MTOM. As MTOM is calculated iteratively, changes in propulsion system mass also impact the other remaining mass groups, hence accounting for the mass snowball effects at the aircraft level. To reflect the state of the art of in-service aircraft, reference values for the structural as well as the systems and equipment mass were derived from simplified mass shares based on publicly available information on the ATR42 aircraft [26,56].

The masses associated with the power plant systems are determined using a more detailed bottom-up approach: while the masses of the propulsive device and the underlying turboshaft engine are calculated from semi-empirical correlations built into SAS, all delta masses due to the HybVer-specific technology case are included based on detailed

parametric assessments performed by the HybVer consortium partners [48,50,51]. The resulting assumptions of the HEP components are summarized in Table 4. The battery system mass is calculated from the battery energy requirement for the aircraft design mission, divided by the prescribed battery system specific energy, and added to the mass budget of systems and equipment. More details on the sizing of the HEP components can be found in Section 3.4.3.

3.2.2. Helicopter

The helicopter geometry and mass is estimated using established semi-empirical handbook methods described in [57,58]. The fuselage wetted area is estimated as a function of MTOM, based on the correlation in [58]. The rotor diameter is calculated from the rotor Disc Loading (DL), the number of blades n_b, as well as the blade chord length c. Both disc loading and chord length can either be specified directly by the user or derived from regressions created from rotorcraft data in [54,59,60]. Similar to the regional aircraft, the helicopter OEM is divided into several main components, including the main rotor mass m_{rot}, structural mass m_{str} (fuselage, nacelles, fuel tank, and landing gear), power train m_{pt} (propulsion system and drive train) and systems and equipment masses m_{sys} (furnishings, avionics, subsystems, and hydraulics). Using a bottom-up approach, each individual item is calculated following the correlations provided in [57,58]. To ensure validity across a wide range of helicopter sizes, the methods are calibrated towards a wide database of over 40 existing rotorcraft [59,60].

All mass components require MTOM as the main input parameter. Furthermore, each mass group depends on a small number of additional inputs. The rotor mass is derived from the previously defined rotor descriptors DL, n_b and c (Equation (3)). The structural mass estimation requires the maximum fuel capacity $m_{fuel,max}$, which is used to determine the tank mass (Equation (4)). This fuel capacity can either be specified by the user or estimated using empirical correlations. The power train mass calculation (excluding the HEP components) depends on the installed power P_{inst} (Equation (5)), which is the total propulsion system power required for Hover Out of Ground Effect (HOGE). It is calculated using a simplified approach provided in [54]. The mass calculation of the HEP components are performed in more detail, as described in Section 3.4.3. Finally, the system and equipment masses additionally require the number of passengers and the fuselage area A_{fus} (Equation (6)):

$$m_{rot} = f(MTOM, DL, n_b, c), \tag{3}$$

$$m_{str} = f\left(MTOM, m_{fuel,max}\right), \tag{4}$$

$$m_{pt} = f(MTOM, P_{inst}), \tag{5}$$

$$m_{sys} = f\left(MTOM, PAX, A_{fus}, P_{inst}\right). \tag{6}$$

3.3. Aerodynamics

3.3.1. Regional Aircraft

The employed version of the SAS framework uses a simple symmetric polar approach based on a straightforward evaluation of the zero-lift, induced and wave drag shares. The wing and fuselage zero drag are calculated by a simple skin friction and form drag method [61]. For the small regional turboprop application case, fully turbulent flow (i.e., zero flow laminarity) was assumed. Parasitic drag effects due to the electric system waste heat rejection are modeled as a function of rejected heat load derived from study results presented in [62]. The operating lift coefficient is deduced from the flight state, the

https://doi.org/10.3390/aerospace13111010

aircraft's Instantaneous Gross Weight (IGW) and the wing reference area. With this, lift-induced drag results from the wing planform and an empirical correlation for Oswald's efficiency factor taken from [56]. All other aircraft drag shares, including the horizontal and vertical tailplanes, aircraft trim and residual parasitic drags, are mapped as a function of the wing zero-drag, with sensitivity to MTOM as a proxy for aircraft size and range capability. During the iterative aircraft sizing, changes in aircraft mass directly affect the overall power requirement and hence propulsion system sizing. For the present study, the impact of increasing engine dimensions on nacelle drag was not considered. Additionally, wave drag effects were neglected due to the relatively low flight speeds of the regional turboprop application.

3.3.2. Helicopter

For the helicopter application, the overall power requirement to overcome the total drag consists of the induced power P_i, the profile power P_0, the parasite power P_p, the climb power P_c and the miscellaneous power P_{misc} [58]:

$$P_{tot} = P_i + P_0 + P_p + P_c + P_{misc}. \quad (7)$$

The individual power components are calculated using the equations from momentum theory and rotorcraft aerodynamics described in [54,58]. The induced power P_i describes the power to generate lift and overcome the weight of the rotorcraft. To account for non-ideal flow conditions, a correction factor is applied [54]. In hover, P_i reaches its maximum and decreases with increasing forward speed, as the mass flow through the rotor disc increases and a smaller induced velocity is required [54]. When operating close to the ground, the induced drag of the helicopter is reduced, which leads to a decrease in induced power (In-Ground-Effect, IGE) [63]. The profile power P_0 is connected to the rotor blade drag. It increases with flight velocity and depends on the blade tip speed, the rotor solidity and the blade profile drag coefficient. The parasite power P_p is needed to counteract the drag of the non-lifting surfaces of the helicopter, such as the fuselage, landing gear and tail structure. A useful parameter for estimating P_p is the equivalent flat plate area [54,64]. It is either specified directly by the user or estimated using empirical correlations. By normalizing the EFPA with the rotor disc area A_{rot}, a non-dimensional metric is obtained that serves as a technology parameter to describe the overall aerodynamic efficiency of the helicopter [64]. The additional power required for climb P_{cl} is calculated using the helicopter mass and climb rate. Lastly, the miscellaneous power P_{misc} accounts for the additional power added due to transmission losses, accessories and the tail rotor. As the resulting total power demand depends on the forward speed, flight altitude, ambient conditions, climb rate and the helicopter's instantaneous gross mass, it is calculated for each flight state along the mission.

3.4. Propulsion System Sizing and Performance Integration

3.4.1. Overall Propulsion System Design

Propulsion system sizing and performance analysis were performed with the MATLAB® R2024b based Aircraft Propulsion System Simulation (APSS) tool [12,15,20,65,66]. It is an in-house design environment built on a modular layout, which enables the easy implementation of novel propulsion system architectures. APSS was validated against industry-standard simulation software such as GasTurb® 12 [67]. Performance synthesis is achieved utilizing standard turbo component maps [68], extensive thermodynamic properties data [69], as well as component-specific sizing laws [70,71]. APSS enables preliminary sizing studies, thermodynamic cycle analyses, as well as extensive parametric modeling capabilities. The framework has been applied to a wide range of conventional and revolutionary propulsion concepts across all engine sizes.

https://doi.org/10.3390/aerospace13111010

For the current investigations, an APSS turboshaft model comprising the CIPH system is set up and depicted in Figure 5. It facilitates a two-shaft architecture, where the high-pressure (HP) shaft connects the high-pressure turbine (HPT) to both the counter-rotating low-pressure compressor (LPC) and the radial high-pressure compressor (HPC). The shaft power generated in the low-pressure turbine (LPT) is transferred to the propeller (regional aircraft) or rotor system (helicopter) through the output shaft. In addition, electrical assistance is integrated into the APSS model via the battery and PMAD system, which distributes electrical power to both motors. Motor A is directly connected to the HP shaft, while Motor B provides electrical power to the counter-rotating compressor.

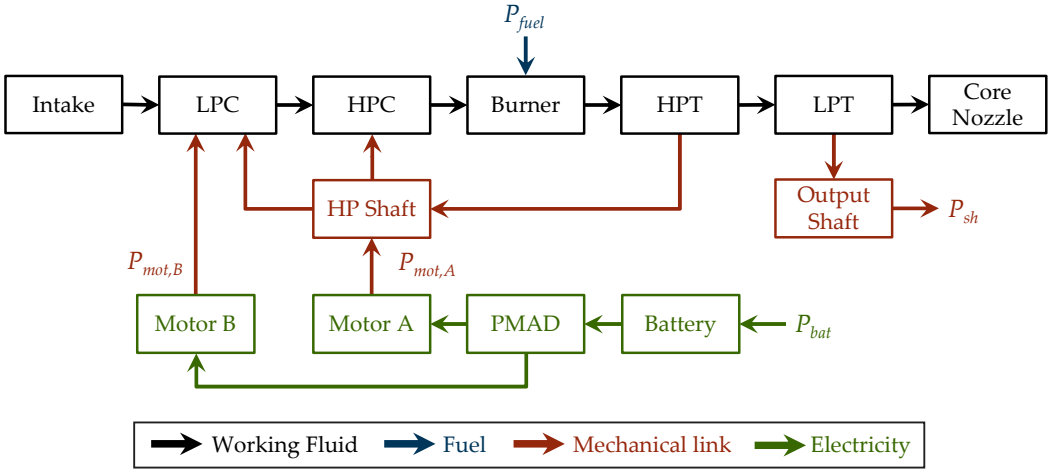


Figure 5. Schematic layout of the APSS propulsion synthesis model for the HybVer electrically assisted turboshaft concept (modified from [15]).

Based on initial estimations for the required power and the design hybridization degree $H_{P,des}$, propulsion system design and performance models are developed for both the conventional baseline and the hybrid electric configuration of each aircraft application. For the targeted EIS in Y2035+, advanced technology settings (e.g., improved turbo component efficiencies) were prescribed. Key cycle parameters, such as the Overall Pressure Ratio (OPR) and the combustor exit temperature T_4, are selected to minimize fuel consumption during cruise conditions while considering different sizing constraints. These include the maximum temperature levels at the turbine inlet, the aerodynamic loading of the compressor stages or the mechanical limitations of the turbine blades [15]. The flow path is sized at the operating point with the highest corrected mass flow. For the regional aircraft application, the sizing point is defined at top-of-climb conditions (M0.4, FL150, ISA+10K) with maximum climb settings. For the helicopter, the flow path is sized at take-off conditions (SLS, ISA+15K).

The specified design hybridization degree $H_{P,des}$ dictates the extent of electrical assistance to the compressor and thus directly affects the sizing of the turbo components. A higher degree of hybridization $H_{P,des}$ reduces the expansion work in the HPT required to drive the compressors, while increasing the expansion work available in the LPT, enabling a downsizing of the core engine. In addition, to provide power to the aircraft subsystems, a constant mechanical power offtake of 65 kW per engine is assumed for the regional aircraft and 30 kW per engine for the helicopter, respectively. Further details on the propulsion system modeling assumptions, including efficiencies, pressure losses, operational limits, geometric settings, as well as the applied sizing heuristics and key performance parameters, are provided in [15].

For integration at the overall aircraft level, the propulsion system performance is evaluated over a range of design and off-design hybridization degrees. First, the efficiency

improvement compared with the non-hybrid baseline propulsion system is determined and used for subsequent aircraft performance calculations. Second, the sizing implications on gas turbine performance, e.g., due to changes in tip clearance losses, is considered, enabling overall aircraft scaling across various power classes.

3.4.2. Consideration of Counter-Rotating Compressor

To assess the implications of the electrically assisted counter-rotating compressor on propulsion system performance, various model extensions have been implemented [15]. An important metric is the rotational speed ratio q_N, defined as the ratio between the tip speeds of the inner (mechanically driven) and outer (electrically driven) rotors [14,72]. It describes how much electrical and mechanical power is provided to the counter-rotating compressor. Applying the speed ratio q_N, relevant counter-rotating compressor design parameters, such as the flow coefficient, work coefficient or the stage pressure ratio, are determined based on the methodology described in [14].

The electric motor shaft power $P_{mot,B}$ supplied directly to the counter-rotating compressor is calculated under consideration of two operational constraints: First, the relative tip speed between the counter-rotating rotors is limited to a maximum relative velocity $\Delta U_{tip,CRC,max}$ in order to minimize the aerodynamic losses due to shock formation and increased pressure losses [15]. Second, to ensure structural integrity of the electric machine, the rotational speed of the electrically driven outer rotors is restricted to avoid excessive centrifugal forces acting on the permanent magnets mounted on the outer rotor diameter. These constraints determine how much $P_{mot,B}$ can be injected into the counter-rotating compressor system. The remaining electrical power supplied by the battery is transferred into the HP shaft via the other electric power train A, hence defining the power split $S_{P,elec}$ between both electric power trains.

$S_{P,elec}$ is evaluated for each operating condition and varies with off-design hybridization and overall power requirement. At high power or high degrees of hybridization, the mechanically driven inner rotors spool up, requiring a reduction in the electrically driven outer rotor speed in order to ensure maximum relative velocity. Due to this, a larger share of the available electrical power is transferred to the HP shaft ($P_{mot,A}$). Conversely, under part-load conditions, additional electrical power must be supplied to the counter-rotating compressor ($P_{mot,B}$) to maintain operability and stable flow conditions. The model allows the electric machine mounted on the HP shaft to operate in both directions. At lower degrees of hybridization, this machine can operate in generator mode, converting excess mechanical shaft power into electrical power to supply the electric machine of the counter-rotating compressor ($P_{mot,B}$).

3.4.3. Hybrid Electric Power Train Sizing

Besides the preliminary design of the gas turbine components, the sizing of the hybrid electric power train components is described in the following section. These components include the battery system, the electric motors, the PMAD system, as well as the TMS required to ensure acceptable operating temperatures of the electric components.

The battery system is sized for the design mission of the respective application case. During the aircraft mission calculation (see Section 3.5), the prescribed design degree of hybridization is assumed to remain constant throughout the main mission segment, whereas no electrical assistance for diversion and reserves is used. The resulting battery system mass is therefore determined from the total required electric energy to complete the design mission and an assumed system-level battery specific energy representative of the projected technology level for an EIS in Y2035+. The selected specific energy implicitly accounts for all conversions from cell to pack and system level as well as limitations on the usable state-of-charge range. Furthermore, a constant battery discharge efficiency was

assumed. To dissipate the battery waste heat, a low-temperature TMS is included and sized using a constant specific mass (see Table 4).

The electrical components are sized based on the peak power requirements achieved at maximum degree of hybridization $H_{P,max}$. The electrical power split between the two electric motors considers the design constraints of the counter-rotating compressor, as described in the previous section. The mass and performance data of the electric machines are based on the work documented in [48,49]. The PMAD system is sized assuming constant values for specific power and efficiency. For the rejection of waste heat generated by the electric machines and the PMAD system, a high-temperature TMS is considered, based on the concept described in [50]. In the current study, the power consumption of both TMSs is neglected.

3.4.4. Consideration of Electric System Failure

In addition to the constraints imposed by the counter-rotating compressor system, further operational limitations need to be considered at the overall propulsion system level. As shown in previous studies (e.g., [12,15–17]), variations in the degree of hybridization (e.g., power extraction or addition) can shift the operating points of the turbo components towards critical limits. Depending on the overall architecture and the type of hybridization (MIPH vs. CIPH), the implications at the propulsion system level vary in severity [16].

For the specific HybVer configuration investigated in this paper, increased electrical assistance leads to higher rotational spool speeds of the turbo components, especially affecting the HPT [15]. In contrast, reduced electrical assistance leads to compressor throttling, which moves the operating points closer to the surge limit and reduces the available surge margin (SM) required for stable compressor operation (cf. [73]). Therefore, the risk of aerodynamic instabilities and compressor stall increases in both LPC and HPC. At the same time, lower hybridization degrees require the gas turbine to compensate for the lower electrical power by increasing fuel flow. This results in higher turbine inlet temperatures, which may lead to lifetime limitation or exceedance of maximum temperature limits. To ensure stable operation and avoid engine shutdown, these limitations therefore impose a minimum degree of hybridization $H_{P,min}$ throughout the mission [15].

Beyond these operational aspects, the risk of electric system failure must be considered. While the probability of a total electric power loss can be reduced by increased redundancy incorporated in the design of the electrical system [74], the propulsion system should nevertheless be capable of safe operation without electrical assistance. At the same time, to avoid oversizing the battery system, the aircraft must also be able to perform non-normal mission segments (e.g., go-around, holding or diversion) without relying on additional electrical power drawn from the batteries. This requirement is especially relevant for regional aircraft applications, where the energy share of reserves and contingencies holds a significant fraction of the total mission block energy [26].

To enable aircraft operation without any electrical assistance and to increase operational flexibility, several design and operational adaptations have been investigated and incorporated into the propulsion system model:

1. Utilization of compressor bleed air extraction to ensure sufficient surge margin and aerodynamic stability.
2. Tailored re-design of turbo components to enhance their operational envelope and increase the overall hybridization potential.
3. Gas turbine oversizing to maintain temperature limitations during critical mission points.

First, the extraction of bleed air from the compressor section improves aerodynamic stability; however, it may lead to increased fuel consumption and temperatures due to the need to compensate for the reduced mass flow through the engine core. Second, adjustments to the turbo component design are implemented in APSS by adjusting the design point within the corresponding performance maps, e.g., further away from the compressor surge line, which can improve operability but may result in reduced component efficiencies. Lastly, oversizing of the gas turbine is achieved by reducing the combustor exit temperature T_4 at the flow path sizing point, resulting in higher mass flows and a lower susceptibility to changes in hybridization. This increases both the minimum and maximum achievable hybridization degree and reduces overall temperatures during normal operation, improving turbine lifetime and NOx emissions. However, oversizing the gas turbine also leads to lower cycle efficiency and increased engine mass, partially offsetting the benefits due to electrical assistance. For the remainder of this paper, the term "with oversizing" is used to describe configurations where all three adaptations were applied, whereas "without oversizing" refers to variants without these mitigation measures.

As all these measures are strongly interdependent in their effect on propulsion system sizing and performance, a full-factorial, multi-dimensional study has been conducted for both application cases. Each study parameter (e.g., bleed air, design T_4, hybridization degree) is varied within predefined ranges, while constraints regarding surge margin, maximum operating temperatures during electric system failure and maximum spool speeds are enforced. The resulting configurations are then evaluated and selected towards minimum fuel consumption during normal cruise operation. The outcome of this study is described in Section 4.1.

3.5. Mission Performance Evaluation

All performance evaluations for the regional application in the present study are conducted at a typical mid-cruise point. Therefore, during aircraft sizing and operational analyses, vehicular IGW is determined at 50% loaded fuel mass $m_{fuel,load}$. The obtained point performance, i.e., IGW, aircraft Lift-to-Drag (L/D) and propulsion system overall efficiency (η_{ov}), at this representative cruise condition is then used as input to the Breguet–Coffin equation, expressed as given in Reference [75], in order to calculate the fuel consumed ($m_{fuel,trip}$) over a prescribed flight distance (ΔR):

$$m_{fuel,trip} = m_{end} \cdot \left(e^{\frac{\Delta R \cdot g}{FHV \cdot L/D \cdot \eta_{ov}}} - 1 \right), \tag{8}$$

where m_{end} is the aircraft gross mass at the end of the considered flight segment, g the gravitational constant, FHV the fuel's lower heating value and η_{veh} the product of L/D and η_{ov}. Assuming the entire mission as a single segment, Δ_m becomes equal to the mission trip fuel. The regional aircraft mission block fuel $m_{fuel,block,REG}$ is the sum of trip fuel $m_{fuel,trip}$ and the fuel used during taxi, landing and take-off $m_{fuel,LTO}$:

$$m_{fuel,block,REG} = m_{fuel,trip} + m_{fuel,LTO}. \tag{9}$$

For the regional aircraft, the total fuel mass for taxi, landing and take-off (LTO) is estimated directly as 0.68% of the aircraft MTOM. This number was derived as an averaged value from flight data of various aircraft types based on results obtained from [76].

For the mission evaluation of the helicopter application, a mission profile consisting of several flight segments such as hover, take-off, climb, cruise, descent and landing is implemented. At each mission segment, different flight conditions (e.g., forward speed, climb rate, altitude, distance and duration) are specified. In this study, a ferry mission was selected as the default mission profile. Other mission profiles such as Oil-And-Gas (OAG), surveillance or Search-And-Rescue (SAR) missions can also be incorporated into the

model. The mission profile is divided into a fixed number of mission points N. At each point, the aerodynamic module is evaluated to determine the required power for the given flight conditions. In the next step, the propulsion system model is evaluated to calculate the associated fuel flow. Finally, the helicopter mission block fuel $m_{fuel,block,HEL}$ is approximated by summing up the engine fuel consumption over each mission point N:

$$m_{fuel,block,HEL} = \sum_{i=1}^{N} n_{eng} \cdot \dot{m}_{fuel,i} \cdot \Delta t_i. \quad (10)$$

where n_{eng} is the number of engines, $\dot{m}_{fuel,i}$ is the engine fuel flow and Δt_i the duration at each mission point. To minimize the discretization error, a sampling number of $N > 200$ mission points was selected. Besides the high sampling density, a segment-based discretization approach has been applied, where mission segments with high gradients in power and fuel consumption (e.g., climb) were discretized with a higher number of sampling points as compared with segments with low gradients. The resulting discretization error in total mission fuel consumption is below 0.05%.

In order to obtain the loaded fuel mass $m_{fuel,load}$ for each application, the fuel mass representing the entirety of contingencies and reserves $m_{fuel,res}$ is added to the mission block fuel $m_{fuel,block}$:

$$m_{fuel,load} = m_{fuel,block} + m_{fuel,res}. \quad (11)$$

For the regional application, an equivalent range of 250 nmi was assumed for contingencies and reserves, while for the helicopter application, the fuel required for 30 min at cruise conditions was added according to [53] (see Table 2).

3.6. Aircraft Iteration and Convergence

Due to the strong coupling between aircraft mass, aerodynamics, propulsion system and mission performance, aircraft sizing and performance is performed iteratively as outlined in Section 3.1. Both the sizing and operational loop (see Figure 4) is initiated by estimating a starting value for MTOM or TOM, respectively. The described modules are then performed in sequence and the updated aircraft mass is obtained by adding the resulting loaded fuel mass $m_{fuel,load}$, OEM and payload, assuming 100 kg per passenger. Mass convergence is reached once the change in (M)TOM falls below a specified convergence criterion.

During the sizing loop (design), the aircraft OEM is updated iteratively and the propulsion system, including the hybrid electric power train, is re-sized for the prescribed design degree of hybridization $H_{P,des}$. As described in Section 3.4.3, the battery energy consumption is derived by maintaining a constant degree of hybridization during the design mission (excluding contingencies and reserves). Hence, with each mass update, different power requirements emerge, directly affecting the resulting fuel and battery system mass.

During the operational (off-design) loop, the component masses remain fixed and only the aerodynamic and propulsion system performance are evaluated iteratively, updating the resulting fuel and Take-Off Mass during each iteration. In parallel to the TOM iteration, the amount of electrical assistance is determined. For this, the off-design degree of hybridization $H_{P,od}$ is iterated to fully utilize the installed battery capacity while remaining within the operational limitations (see Section 3.4) posed by the propulsion system. During off-design calculation, the battery Depth of Discharge (DoD) is used to monitor the share of available battery energy consumed over the mission. It is defined as

$$DoD = \frac{E_{mis}}{E_{tot,use}}, \quad (12)$$

where E_{mis} is the electrical energy consumed during the mission and $E_{tot,use}$ is the total usable energy capacity of the battery. Depending on the mission payload and range requirements, two operating conditions may occur. On longer missions, the installed battery capacity can be distributed over a longer period of time. This results in lower off-design hybridization degrees that remain within the allowable limits and enable a full depletion of the battery's usable energy capacity (DoD = 100%). On shorter missions, however, utilizing the same installed battery energy within a shorter mission duration requires a higher electrical power. This increases the off-design hybridization degree until the maximum hybridization limit $H_{P,max}$ is reached and the electric machines operate at their maximum rated sizing power. In this case, the usable battery capacity can no longer be fully utilized during the mission, resulting in a DoD < 100%. Energy convergence is reached when the change in DoD lies within a prescribed tolerance and a feasible off-design hybridization degree has been determined.

3.7. Validation of Framework

To show the validity of the presented methodology across different aircraft classes, a set of representative fixed- and rotary-wing aircraft is designed and compared with publicly available data.

Next to the validation cases presented in [44], two additional fixed-wing aircraft are considered for the validation of the SAS framework: a regional ATR42-600 as well as a short-to-medium range A320-200. Both aircraft are sized based on TLARs derived from literature data [26,77]. The sizing and scaling methodology described in Section 3.1 was applied and the validation results are summarized in Table 5. Recalculation of the ATR42-600 with 48 PAX at 95 kg each and a design range of 716 nmi yielded very good agreement, with all main aircraft parameters deviating up to 1% from the public reference data [26] and MTOM matching as close as 0.7%. As a second validation case, an A320-200 with 150 PAX at 100 kg each and a design range of 2350 nmi is modeled, showing similar agreement for the key aircraft parameters. Compared with the reference data [77], MTOM only deviates by 0.14%, while the design fuel is underestimated by 2.7%.

Table 5. Validation of the fixed-wing aircraft sizing methodology against reference data for the ATR42-600 and A320-200.

Parameter	Unit	ATR42-600			A320-200		
		Calculated	Ref. Data	Delta (%)	Calculated	Ref. Data	Delta (%)
Design payload	kg	-	4560	Input	-	15,000	Input
Design range	nmi	-	716	Input	-	2350	Input
Wing loading	kg/m²	-	340	Input	-	600	Input
Aspect ratio	-	-	11	Input	-	9.5	Input
MTOM	t	18.5	18.6	−0.69	73.4	73.5	−0.14
OEM	t	11.5	11.6	−0.68	41.7	41.6	0.76
Design fuel	t	2.39	2.37	1.03	16.7	17.2	−2.69
Wing area	m²	54.3	54.5	−0.32	122	122	−0.06
Wing span	m	24.5	24.5	0.10	34.1	34.1	−0.03

Overall, the resulting MTOM, OEM and wing dimensions are in good alignment with the aircraft models and the reference data, with the highest deviations occurring for the design fuel, possibly due to uncertainties in estimating the overall aircraft drag. However, these deviations are considered within an acceptable range for the scope of the current study. As additional cross-checks, the reference, baseline and conservative hybrid electric aircraft configurations from the H2020 project IMOTHEP (cf. [26]) were recalculated,

indicating an excellent level of plausibility of the predicted aircraft mass and design mission fuel terms.

Similar to the fixed-wing aircraft, two representative rotary-wing aircraft are selected to validate the HOVER framework, covering different power and utility classes. Based on publicly available data [59,78–80], the light utility helicopter MBB Bo 105 CB and the super-medium transport helicopter AW189K are recalculated using the methodology described above. For both helicopters, the design payload is obtained by subtracting the OEM and the design fuel mass from the MTOM, due to the limited availability of helicopter design payload data. The results of the validation are summarized in Table 6.

Table 6. Validation of the rotary-wing aircraft sizing methodology against reference data for the Bo 105 CB and AW189K.

Parameter	Unit	Bo 105 CB			AW189K		
		Calculated	Ref. Data	Delta (%)	Calculated	Ref. Data	Delta (%)
Design payload	kg	-	761	Input	-	1346	Input
Design range	km	-	656	Input	-	750	Input
Disc loading	kg/m²	-	26.5	Input	-	51.4	Input
Rotor diameter	m	-	9.84	Input	-	14.6	Input
EFPA	m²	-	1.00	Input	-	2.34	Input
MTOM	t	2.52	2.50	0.64	8.57	8.60	−0.37
OEM	t	1.29	1.28	1.14	5.66	5.63	0.53
Design fuel	kg	461	460	0.20	1649	1661	−0.74

Overall, only slight deviations from the reference data can be observed. The largest difference is observed for the OEM of the Bo 105 at 1.14%, while for the AW189K, all parameters deviate by less than 1%. The validation results therefore indicate a high level of plausibility of the implemented methodology, allowing further usage for the subsequent sizing and performance studies.

4. Results

4.1. Propulsion System Performance

To better understand the implications at the aircraft level, key propulsion system characteristics are discussed first. For this, the baseline and hybrid electric propulsion systems for each aircraft configuration were preliminarily designed and investigated as described in [15]. Next, a multi-point design study, considering the adaptation measures described in Section 3.4.4, is performed to identify a best and balanced design that enables operation without electrical assistance. The results of this study for the regional application are summarized in Figure 6, displaying the variation in key propulsion system parameters relative to the baseline engine as a function of the design degree of hybridization $H_{P,des}$. These parameters include the combustor exit temperature $T_{4,des}$ at the flow path sizing point, the resulting gas turbine (GT) mass and the power-specific fuel consumption (PSFC) during cruise conditions $PSFC_{cr}$.

$T_{4,des}$ is used as a design parameter to control the sizing of the gas turbine. Decreasing $T_{4,des}$ will result in lower available enthalpy and a reduced specific work extraction within the turbines. To compensate for this, the engine mass flow must increase, resulting in a larger gas turbine size and weight. Furthermore, lower $T_{4,des}$ also reduces the thermal efficiency of the thermodynamic cycle, negatively affecting fuel consumption.

Figure 6 displays two variants of the hybrid electric regional aircraft (REG-HYB) propulsion system relative to the engine of the baseline aircraft (REG-BAS). The first one does not include any design adaptations to account for electric system failure (without oversizing). The second variant considers these measures, including gas turbine oversizing

through a reduction in $T_{4,des}$ (with oversizing). The corresponding ranges and their quantitative impact on PSFC and GT mass are provided in absolute values in Table A1.

For the variant without oversizing, increasing the design hybridization degree $H_{P,des}$ continuously reduces the GT mass. Since part of the compressor work is replaced by the electric power train, less thermal work extraction is needed in the turbines and the gas turbine can be downsized accordingly. Additionally, power-specific fuel consumption $PSFC_{cr}$ improves substantially, as the highly efficient electric power train is utilized more [12,14,15].

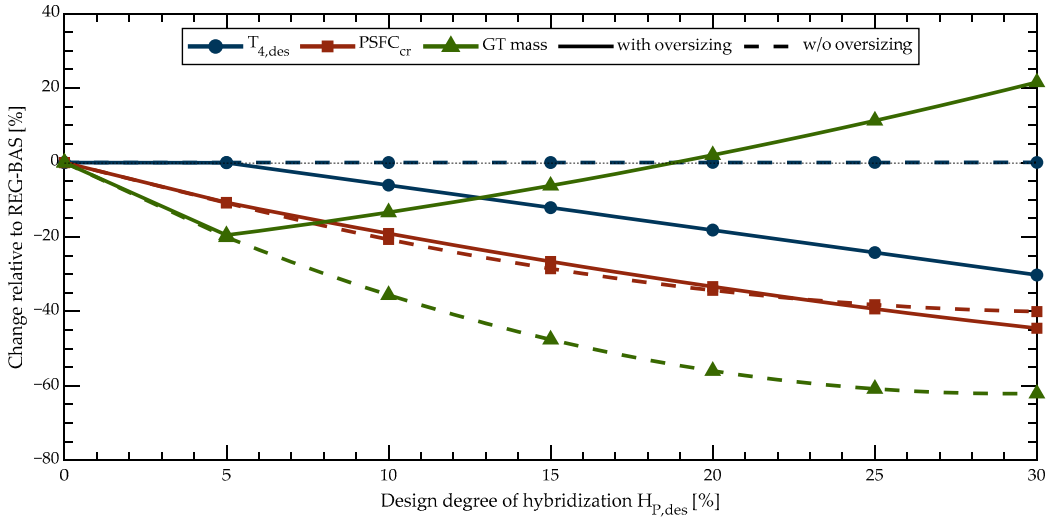


Figure 6. Impact of gas turbine oversizing and design degree of hybridization on key propulsion system parameters relative to the baseline engine (regional aircraft application).

For the variant with mitigation measures towards electric system failure, no reduction in $T_{4,des}$ is required up to $H_{P,des} \leq 5\%$. In these cases, other adaptations such as handling bleed or design point adjustments within the corresponding performance maps are sufficient to compensate for a total loss of electric power. Even in the event of electric power loss during hot take-off, the engine temporarily remains within its red line temperature limits. Hence, only minor deviations compared with the non-oversized variant occur, showing similar trends regarding GT mass and $PSFC_{cr}$.

For hybridization degrees above $H_{P,des} > 5\%$, reductions in $T_{4,des}$ become necessary to stay within the operational limits in case of electric system failure. As more electrical power must be compensated with increasing $H_{P,des}$, larger gas turbine oversizing is required. This leads to a continuous increase in GT mass, reaching around 20% above the baseline engine mass at $H_{P,des} = 30\%$. The reduction in $T_{4,des}$ also affects the thermal efficiency of the cycle. Compared with the variant without oversizing, $PSFC_{cr}$ increases by up to 2% at around $H_{P,des} = 15\%$. However, with growing size discrepancy at higher hybridization degrees ($H_{P,des} > 23\%$), this trend reverses. As the blade tip clearance losses become increasingly dominant with smaller core size, the turbo component efficiencies and the $PSFC_{cr}$ of the non-oversized variant deteriorate.

Since the same overall trends are observed for the helicopter engine, the propulsion system results are shown only for the regional application. The main difference lies in the performance penalty associated with the various mitigation measures. For the helicopter engine, the resulting $PSFC_{cr}$ increases by up to 9% compared with the variant without any measures. This is mostly caused by the larger adjustments required in handling bleed and turbo component maps.

After discussing the impact of failure-mitigation measures on key propulsion system parameters, the off-design performance characteristics of the hybrid electric propulsion

system are investigated. Unless stated otherwise, all following results refer to the oversized propulsion system with robustness towards electric system failure.

Figure 7a displays the PSFC improvements of the REG-HYB propulsion system relative to the REG-BAS for varying design hybridization degrees $H_{P,des}$ and off-design hybridization degrees $H_{P,od}$. In addition, the minimum and maximum hybridization degrees $H_{P,min}$ and $H_{P,max}$ are indicated for each design hybridization degree. Due to the previously described reduction in $T_{4,des}$ and the resulting gas turbine oversizing, operation without electrical assistance ($H_{P,min}$ = 0%) can be maintained for all design hybridization degrees.

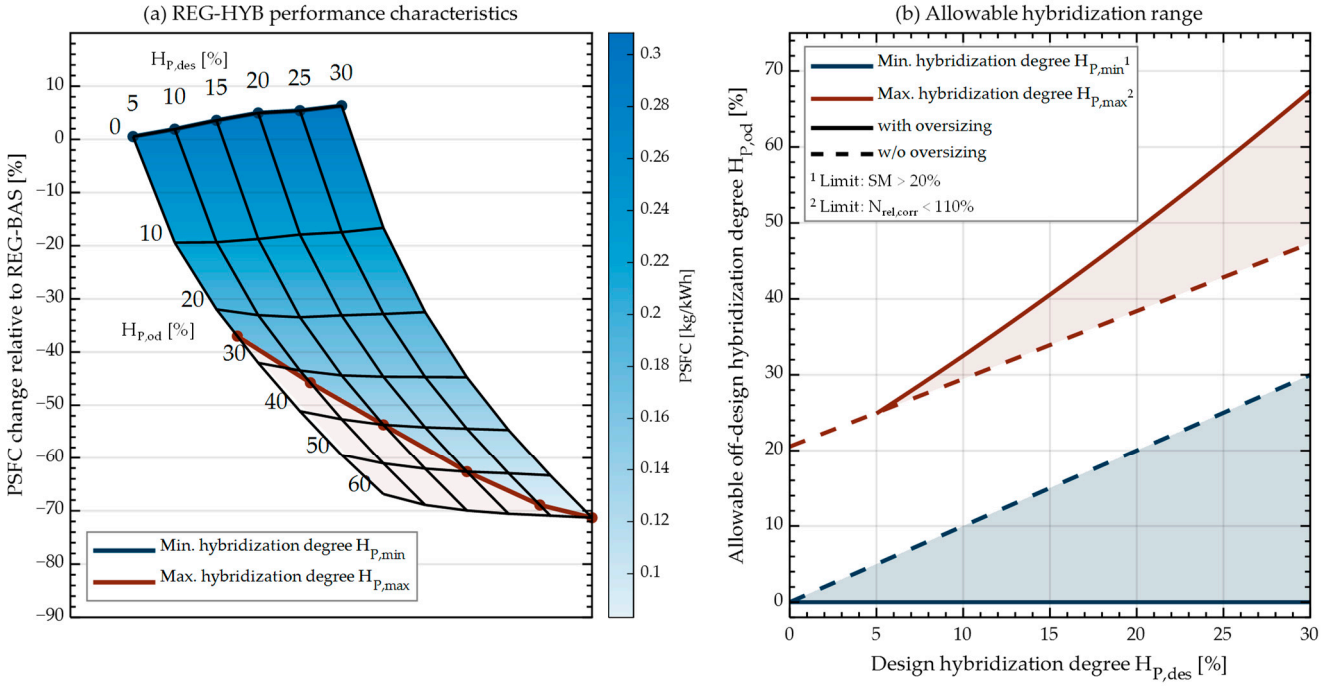


Figure 7. Hybrid electric propulsion system performance characteristics: (**a**) impact of design and off-design hybridization on relative PSFC (with oversizing) and (**b**) impact of gas turbine oversizing on the allowable off-design hybridization range (regional aircraft application).

With changing values in $H_{P,des}$, only minor changes in PSFC can be observed. These differences result from the previously described mitigation measures, slightly decreasing the cycle efficiency and shifting the operating point within the turbo component maps. In contrast, increasing the off-design hybridization degree $H_{P,od}$ leads to significant reductions in PSFC relative to the baseline engine, caused by the higher utilization of the hybrid electric power train. These improvements are, however, limited by the operational constraints of the propulsion system, requiring the operational hybridization degrees to remain within $H_{P,od} < H_{P,max}$. It can be observed that with increasing $H_{P,des}$, larger values of $H_{P,max}$ are achievable. Since the propulsion system is sized for a prescribed design hybridization degree $H_{P,des}$, increasing $H_{P,des}$ shifts the associated feasible off-design range accordingly. As a result, the maximum achievable PSFC improvement increases from around −35% at $H_{P,des}$ = 5% to more than −70% at $H_{P,des}$ = 30%. At the propulsion system level, this favors higher design hybridization degrees. However, at the aircraft level, the increase in electrical energy and power results in larger battery and electrical component masses.

The increase in $H_{P,max}$ with growing $H_{P,des}$ is depicted more clearly in Figure 7b, highlighting the effect of oversizing on the off-design hybridization potential. As explained in more detail by [15,16], the feasible hybridization range of the proposed propulsion system is limited on both ends by operational constraints. At lower hybridization degrees ($H_{P,od} < H_{P,des}$), the minimum hybridization degree $H_{P,min}$ is restricted by surge margin constraints

of the HPC and LPC, requiring a minimum surge margin of 20%, as well as by maximum operating temperatures. For higher hybridization degrees ($H_{P,od} > H_{P,des}$), the maximum hybridization degree $H_{P,max}$ is limited by the allowable relative corrected spool speeds $N_{rel,corr}$ of the HPT and LPT. The maximum permissible value is 110% of its respective design corrected spool speeds, as defined by the selected representative turbine maps found in [68].

Without the mitigation measures described in Section 3.4.4, the feasible hybridization range is very narrow. Even though the whole range shifts towards higher hybridization levels with growing $H_{P,des}$, the allowable deviation from the design point remains limited. As a result, the propulsion system cannot operate without electrical assistance and only allows a small increase in hybridization during off-design operation. On the other hand, implementing oversizing measures significantly expands the allowable hybridization range (see Figure 7b). Due to the larger size of the gas turbine components, the engine becomes less sensitive to changes in hybridization. Thus, the corresponding shifts of the operating points within the turbo component maps are less severe, allowing a bigger offset from $H_{P,des}$ before operational limits are reached. This not only enables operation without electrical assistance ($H_{P,min} = 0\%$) but also increases the maximum hybridization degree $H_{P,max}$ compared with the variant without oversizing.

Despite the drawbacks that oversizing causes in terms of GT mass and PSFC (see Figure 6), the resulting increase in operational flexibility enables significantly higher off-design hybridization degrees. During aircraft operation, this advantage can be exploited particularly on shorter routes, where higher hybridization levels can be achieved by fully utilizing the installed battery capacity. The resulting effects on aircraft sizing and performance are presented in the following sections.

4.2. Regional Aircraft Sizing and Performance

In this section, the integrated aircraft-level performance results for the regional aircraft application are presented. For this purpose, the propulsion system characteristics described in the previous section are incorporated into the overall framework. All following results consider propulsion systems with oversizing, enabling continuous aircraft operation without electrical assistance (e.g., during alternate mission) and hence increasing robustness to electric system failure. To determine the optimum HEP sizing, the design degree of hybridization $H_{P,des}$ is varied between 0% and 30%. For each design point, a complete aircraft sizing is performed. In addition, the battery system specific energy is varied between 400 and 600 Wh/kg to evaluate the influence of future battery technology on aircraft level.

Figure 8 compares the mission fuel burn of the REG-HYB relative to the REG-BAS for both the design mission (a) and the typical mission (b). For the design mission at 400 nmi and full payload, increasing design degrees of hybridization $H_{P,des}$ results in larger installed battery capacities and therefore higher battery masses. This results in increased aircraft Take-Off Masses and overall propulsion system power requirements. At the same time, increased hybridization improves the propulsion system efficiency and reduces specific fuel consumption (see Figure 7a). Hence, at the overall aircraft level, the mission fuel burn depends on the trade-off between the HEP mass penalty and the propulsion system efficiency improvement.

For a battery specific energy of 400 Wh/kg, the additional masses outweigh the efficiency gains, resulting in little to no improvement in design mission fuel consumption compared with the baseline aircraft. With increasing battery specific energy, the HEP mass penalty is reduced and fuel burn improvements can be achieved. With an optimistic technology assumption of 600 Wh/kg, a maximum design fuel burn change of up to −6% is obtained.

https://doi.org/10.3390/aerospace13111010

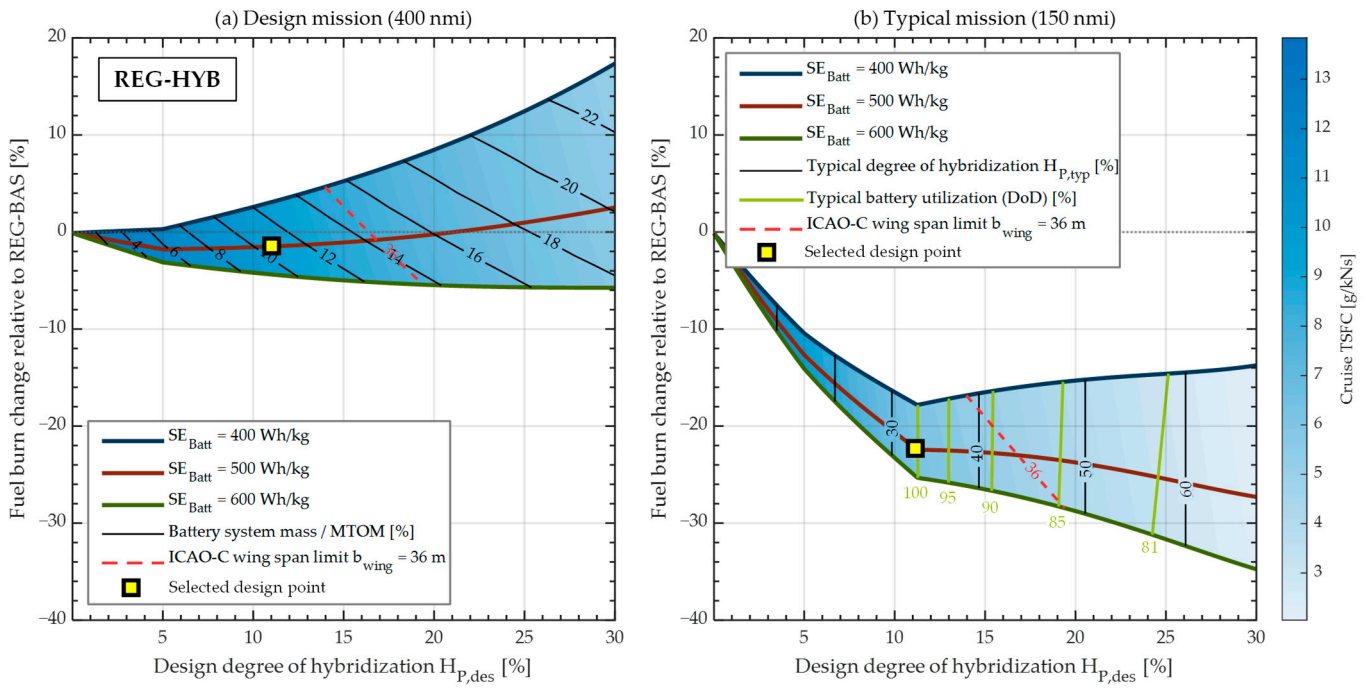


Figure 8. Regional hybrid electric aircraft sizing for varying design degrees of hybridization and battery technology assumptions, with corresponding relative block fuel for (**a**) the design mission at $H_{P,des}$ and (**b**) the typical mission at $H_{P,typ}$ (with maximum feasible battery utilization).

A substantially different trend can be observed for the typical mission (150 nmi), as shown in Figure 8b. Although the aircraft and propulsion system is sized for the design mission, the shorter mission duration enables significantly higher operational hybridization by fully utilizing the installed battery capacity during flight. The achieved mission hybridization $H_{P,typ}$ is significantly higher than for the design mission, resulting in larger efficiency improvements and lower mission fuel consumption.

With increasing $H_{P,des}$, the installed battery capacity grows, allowing for higher typical hybridization degrees $H_{P,typ}$. The relative fuel burn initially decreases for all investigated battery technologies. However, at a specific value of $H_{P,des}$, a kink can be observed. At this point, the typical hybridization degree reaches its maximum allowable value $H_{P,typ} = H_{P,max}$, limited by the maximum spool speeds of the turbo components [15]. Note that $H_{P,max}$ is not constant, but growing with $H_{P,des}$ (as shown in Figure 7b). However, beyond this kink point, the battery cannot be fully utilized over the course of the typical mission, resulting in a reduced battery utilization (DoD < 100%).

The impact of further increasing the battery size beyond this point depends strongly on the assumed battery technology. At 400 Wh/kg, the trend reverses and the relative fuel burn deteriorates. In this case, the optimum design is at the kink point with a fuel burn reduction of around 18% at $H_{P,des}$ = 11%. For battery specific energies of 500 Wh/kg and above, a tipping point is reached, where increased hybridization overcompensates the HEP mass penalty, despite operating at $H_{P,max}$. This shifts the optimum towards the highest investigated hybridization levels ($H_{P,des}$ = 30%).

To identify a best-and-balanced aircraft design point, additional sizing constraints must be considered at the aircraft level. Increasing $H_{P,des}$ leads to larger aircraft masses and thus larger wing size. To remain within the ICAO code C airport category, the aircraft wing span b_{wing} must not exceed 36 m [81]. A larger wing span would limit the operational flexibility, as the number of airports that can accommodate such aircraft is reduced. The selected aircraft design point at 500 Wh/kg is thus set at the kink point with $H_{P,des}$ = 11%.

Further increasing $H_{P,des}$ would only marginally improve typical mission fuel burn at the cost of higher battery mass.

The resulting aircraft design and mission performance parameters of the REG-BAS and REG-HYB aircraft can be found in Table 7. Additionally, Figure 9 displays the mass breakdown of both aircraft in absolute values. Compared with the baseline aircraft, MTOM increases by 48%, while OEM grows by 75%. The increase in mass is attributed to the higher HEP mass, specifically the battery mass, contributing 2740 kg to the overall aircraft mass. As a result of this, the aircraft thrust demand increases as well. The applied oversizing measures reduce the cruise combustor exit temperature $T_{4,cr}$ by 7%. Furthermore, the larger wing to support the additional mass leads to a slight improvement in aerodynamic efficiency of the aircraft, as represented by the lift-to-drag ratio.

Table 7. Regional aircraft design and mission performance characteristics for the baseline (REG-BAS) and hybrid electric (REG-HYB) variant.

Parameter		Unit	REG-BAS	REG-HYB	Delta (%)
MTOM		kg	17,400	25,700	48%
OEM		kg	10,900	19,100	75%
Cruise thrust		kN	11.5	15.6	35%
L/D		-	13.8	15.2	11%
Wingspan		m	26.8	32.5	22%
$T_{4,cr}$		K	1569	1455	−7%
Battery mass		kg	-	2740	-
Design mission	Payload	kg	5000	5000	-
	Range	nmi	400	400	-
	Degree of hybridization	%	-	11	-
	TSFC	g/kNs	11.9	8.4	−29%
	Block fuel	kg	941	928	−1%
	Energy	MWh	11.2	12.5	11%
Typical mission	Payload	kg	5000	5000	-
	Range	nmi	150	150	-
	Degree of hybridization	%	-	34	-
	TSFC	g/kNs	11.9	5.5	−53%
	Block fuel	kg	420	328	−22%
	Energy	MWh	5.0	5.3	5%

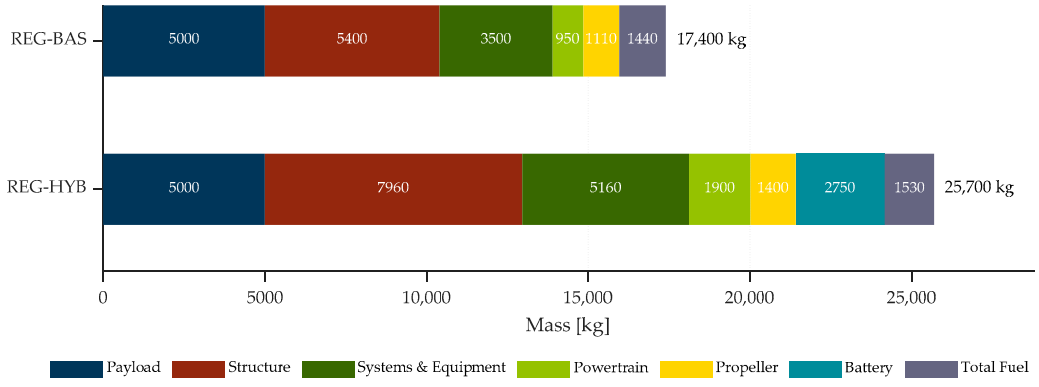


Figure 9. Mass breakdown of the baseline (REG-BAS) and hybrid electric (REG-HYB) regional aircraft.

For the design mission, the Thrust-Specific Fuel Consumption (TSFC) is reduced by around 29%. This improvement can be explained by two main reasons: First, electrical assistance of the compressor ($H_{P,des}$ = 11%) benefits from the high efficiency of the electric power train. Second, the increased engine size improves the thermal efficiency of the gas

turbine due to the reduced impact of blade tip clearance losses. Overall, all effects combined result in an aircraft fuel burn reduction of 1% for the design mission.

For the typical mission, full battery utilization on the shorter mission increases the hybridization degree to $H_{P,typ}$ = 34%. This amounts to almost three times the design hybridization, reducing the TSFC by 53% and leading to a typical mission fuel burn reduction of 22% compared with the baseline aircraft.

The total energy consumption of the hybrid regional aircraft compared with the baseline aircraft for different hybridization levels and battery technologies is shown in Figure A1. Despite the reduction in fuel consumption, the overall energy consumption increases by around 11% for the design mission and 5% for the typical mission, strongly driven by the increased aircraft mass.

4.3. Helicopter Sizing and Performance

While the regional aircraft showed substantial fuel burn improvements for the typical mission by fully utilizing the battery capacity, the potential of the proposed parallel HEP system also depends on the aircraft application. To shed light on this, the same aircraft-level investigations are performed for the helicopter application. All results were conducted with oversizing of the propulsion system, to account for electric system failure and enable operation at zero electrical supply power.

Compared with fixed-wing aircraft, rotorcraft applications are fundamentally different in many ways. First, conventional helicopters require continuous rotor lift during the mission, limiting the maximum achievable range and resulting in a smaller spread between the design and typical range. This may reduce the utilization potential of the battery on shorter missions. Second, helicopters require much higher power levels during take-off and climb, as the rotor must provide most of the required lift in those low-speed regimes. Compared with a fixed-wing aircraft, this leads to a larger propulsion system power lapse between take-off and cruise [63]. Third, due to the combination of both previous effects, helicopters spend a shorter mission share in the efficient low-power cruise condition and a larger share in high-power segments such as hover and climb. Finally, rotorcraft are generally more affected by additional mass increases, which may limit the achievable battery size.

The implications of these effects on the relative mission fuel burn of the hybrid electric helicopter (HEL-HYB) compared with the baseline helicopter (HEL-BAS) is shown in Figure 10. On the left, the design mission (200 nmi) results are displayed; on the right, the typical mission (100 nmi). As for the regional application, the performance characteristics of the oversized helicopter propulsion system are considered in the results to enable operation without electrical assistance.

For the design mission, the helicopter mission fuel burn reacts much more strongly to increasing design hybridization and hence HEP mass than the regional aircraft. As mentioned before, additional helicopter mass has a larger effect on MTOM and overall power requirement, resulting in a stronger increase in mission energy demand and hence a steeper fuel burn degradation with rising $H_{P,des}$. The strong increase in overall power demand with rising helicopter mass also impacts the battery sizing, as the resulting battery mass fraction relative to MTOM grows more rapidly compared with the regional aircraft (see Figure 8a). Additionally, the propulsion system efficiency is impacted by the oversizing effects, which severely increases the PSFC compared with the engine configuration without oversizing. As a result, no fuel burn benefit can be achieved during the helicopter design mission for all investigated battery technologies.

To limit the HEP mass penalty, the electric machines and PMAD system are sized for the cruise power of the typical mission rather than the significantly higher HOGE power demand. Thus, the electric machines operate at the design hybridization level during

high-power mission segments, while higher hybridization levels can be achieved during cruise operation.

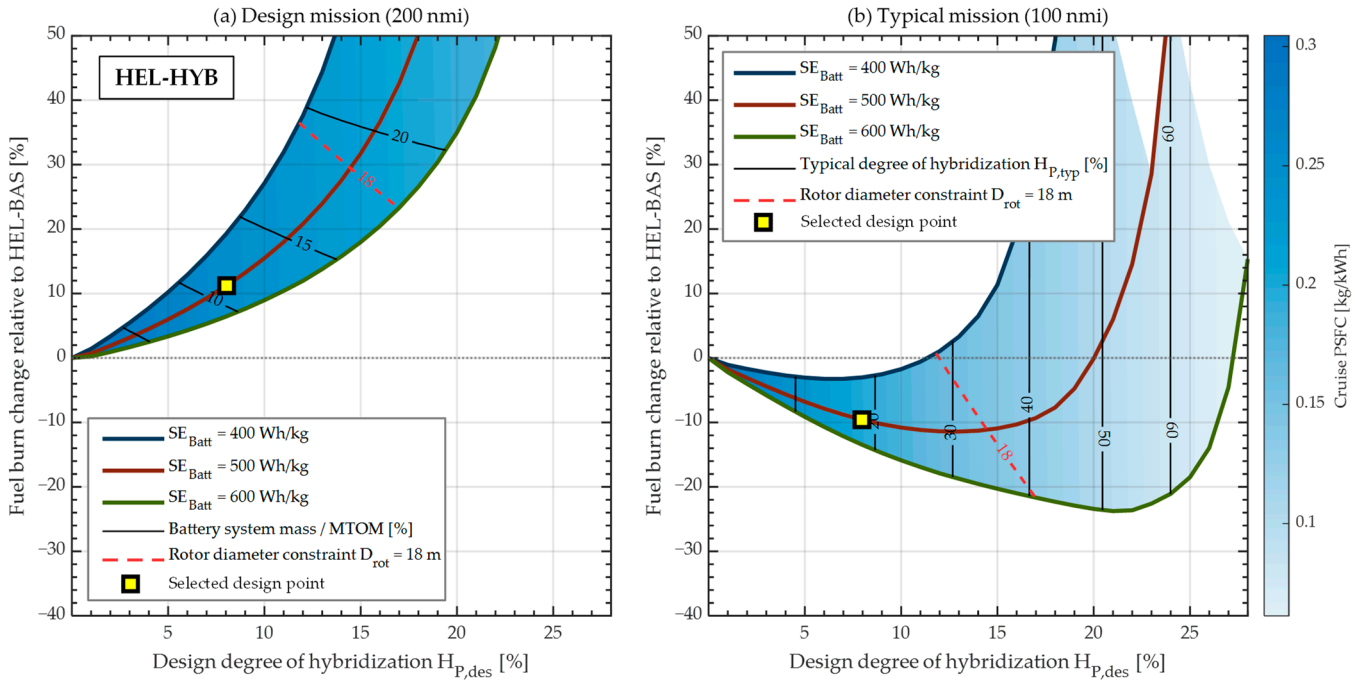


Figure 10. Hybrid electric helicopter sizing for varying design degrees of hybridization and battery technology assumptions, with corresponding relative block fuel for (**a**) the design mission at $H_{P,des}$ and (**b**) the typical mission at $H_{P,typ}$ (with maximum feasible battery utilization).

The typical mission performance of the hybrid electric helicopter is shown in Figure 10b. Similar to the regional aircraft, the installed battery capacity is utilized to increase the operational hybridization degree ($H_{P,typ}$) during the shorter mission. Compared with the design mission, where the HEP mass penalty dominates, the higher hybridization degrees improve the propulsion system efficiency and hence mission fuel burn. Depending on the assumed battery specific energy, significant fuel burn improvements relative to the baseline helicopter can be achieved. For all battery technologies, a clear fuel burn optimum can be seen. Up to this point, increasing battery capacity leads to further fuel burn reductions. Beyond the optimum, however, the fuel burn benefits deteriorate, as the additional HEP masses overcome the efficiency gains from the hybrid electric propulsion system.

In contrast to the regional aircraft results (see Figure 8b), no kink point is visible in the typical mission fuel burn trends. This can be explained by the fact that the helicopter never reaches its maximum hybridization degree $H_{P,max}$ during the typical mission. Due to the relatively small range gap between the design and typical mission, the battery capacity cannot be fully utilized within the available mission duration. Furthermore, the larger share of hover and climb segments reduces the time spent in the highly hybridized cruise segment, limiting the overall electric energy drawn from the battery compared with the regional aircraft.

Selecting a suitable design point for the hybrid electric helicopter is challenging, as the helicopter results show a strong dependence on the actual mission range. The actual potential of the proposed propulsion concept depends on how the aircraft is utilized in service and which payload–range requirements are most frequently encountered. Furthermore, all mission evaluations are assumed to operate at maximum payload. This represents a conservative assumption, as in practice, many helicopter missions are operated at reduced payload, which could improve the achievable benefits of electrical assistance. In addition, a geometric constraint is imposed on the helicopter design. Similar to the wing

span constraint of the regional aircraft, the rotor diameter of the helicopter must remain within a reasonable range. Based on the rotor dimensions of existing helicopters used for offshore operations, the maximum rotor diameter is assumed to be 18 m [82].

Assuming an equal weighting of the design and typical missions, the selected helicopter design point for a battery specific energy of 500 Wh/kg is chosen at $H_{P,des}$ = 8%, resulting in a similar fuel burn reduction for the typical mission and a fuel burn penalty for the design mission. Increasing $H_{P,des}$ even further would result in only moderate typical mission improvements, while significantly worsening the design mission performance. The key design and performance specifications of the selected hybrid helicopter (HEL-HYB) compared with the baseline helicopter (HEL-BAS) are shown in Table 8. The mass breakdown of both helicopter applications is displayed in Figure 11.

Table 8. Helicopter design and mission performance characteristics for the baseline (HEL-BAS) and hybrid electric (HEL-HYB) variant.

Parameter		Unit	HEL-BAS	HEL-HYB	Delta (%)
MTOM		kg	6710	9180	37%
OEM		kg	4210	6580	56%
HOGE power		kW	1040	1500	44%
EFPA		m^2	1.69	2.08	23%
Rotor diameter		m	14.6	16.3	11%
$T_{4,cr}$		K	1562	1478	−5%
Battery mass		kg	-	1030	-
Design mission	Payload	kg	1900	1900	-
	Range	nmi	200	200	-
	Degree of hybridization	%	-	8	-
	PSFC	kg/kWh	0.30	0.25	−17%
	Block fuel	kg	443	492	11%
	Energy	MWh	5.3	6.4	21%
Typical mission	Payload	kg	1900	1900	-
	Range	nmi	100	100	-
	Degree of hybridization	%	-	18	-
	PSFC	kg/kWh	0.30	0.20	−33%
	Block fuel	kg	231	209	−10%
	Energy	MWh	2.8	3.0	9%

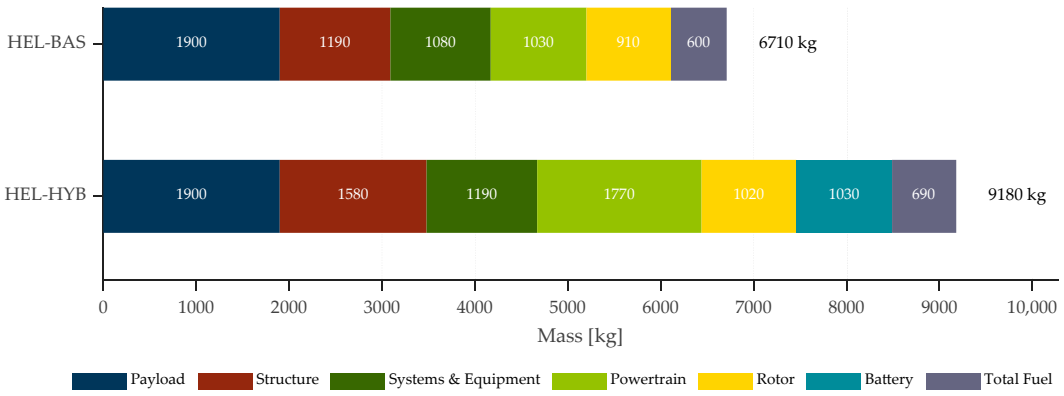


Figure 11. Mass breakdown of the baseline (HEL-BAS) and hybrid electric (HEL-HYB) helicopter.

Compared with the baseline helicopter, MTOM grows by 37% and OEM increases by 56%. The mass increase is caused by the higher HEP mass, with the battery system alone contributing 1030 kg to the overall helicopter mass. This directly leads to an increase in power demand as well. Furthermore, the larger helicopter size increases fuselage drag, as expressed by the equivalent flat plate area.

For the design mission, the PSFC is reduced by around 17% due to the benefits from hybridization ($H_{P,des}$ = 8%). However, as mentioned before, mission fuel consumption of the hybrid helicopter is increased by 11% for the design mission. For the typical mission, the shorter mission increases the operational hybridization degree to $H_{P,typ}$ = 18%. This results in a PSFC reduction of 33%, leading to a typical mission fuel burn reduction of 10% compared with the baseline helicopter.

The overall energy consumption of the hybrid helicopter for different battery technologies and hybridization levels is provided in Figure A2. Compared with the baseline application, the overall energy consumption increases by approximately 21% for the design mission and 9% for the typical mission.

4.4. Regional Aircraft Design Range Sensitivity

As shown in the previous sections, substantial fuel burn reductions can be achieved for the typical mission through increased hybridization. In the next step, the influence of the selected aircraft design range on the overall aircraft performance is investigated. Since the regional aircraft has shown a bigger overall potential than the helicopter application, the following sensitivity study focuses only on the regional aircraft. The objective is to understand how different design ranges influence the overall aircraft and propulsion system sizing, how the optimum degree of hybridization changes and how these effects impact fuel efficiency for both typical and design missions. This provides answers towards the scalability of the proposed parallel HEP system towards larger regional aircraft applications.

In the study, the aircraft design range is varied together with the battery specific energy and the design degree of hybridization $H_{P,des}$. Each combination represents a completely new aircraft design and therefore results in a different aircraft geometry, mass breakdown, propulsion system sizing and mission performance. Thus, the following results do not simply show different off-design missions for a fixed aircraft, but the performance of various newly sized aircraft tailored to their respective design ranges.

Figure 12a shows the typical mission fuel burn improvement of the REG-HYB relative to the REG-BAS aircraft over different aircraft design ranges for a battery specific energy of 500 Wh/kg. Similar to the previous analysis, the design degree of hybridization $H_{P,des}$ is varied to adjust the installed battery capacity and the corresponding HEP size. As discussed in Section 4.2, the typical mission fuel burn initially improves with rising design hybridization, until the maximum achievable hybridization degree $H_{P,max}$ is reached (kink point). Beyond this point, the battery can no longer be fully utilized during the mission and further increases in battery size lead to diminishing or even reverse fuel burn trends.

As can be seen in Figure 12a, the location of the kink points changes considerably with increasing design range. For larger design missions, the kink occurs at lower values of $H_{P,des}$. This can be explained by the increasing spread between the design and the typical (150 nmi) mission range. If the battery system is sized for a longer design mission, more electrical power can be extracted during the shorter typical mission. This increases the operational hybridization degree, causing the hybridization limit to be hit at a lower $H_{P,des}$. For smaller design ranges, the opposite trend can be observed. As the difference between the design and typical mission ranges decreases, the operational hybridization degree during the typical mission is reduced and the hybridization limit is reached at a higher value of $H_{P,des}$.

https://doi.org/10.3390/aerospace13111010

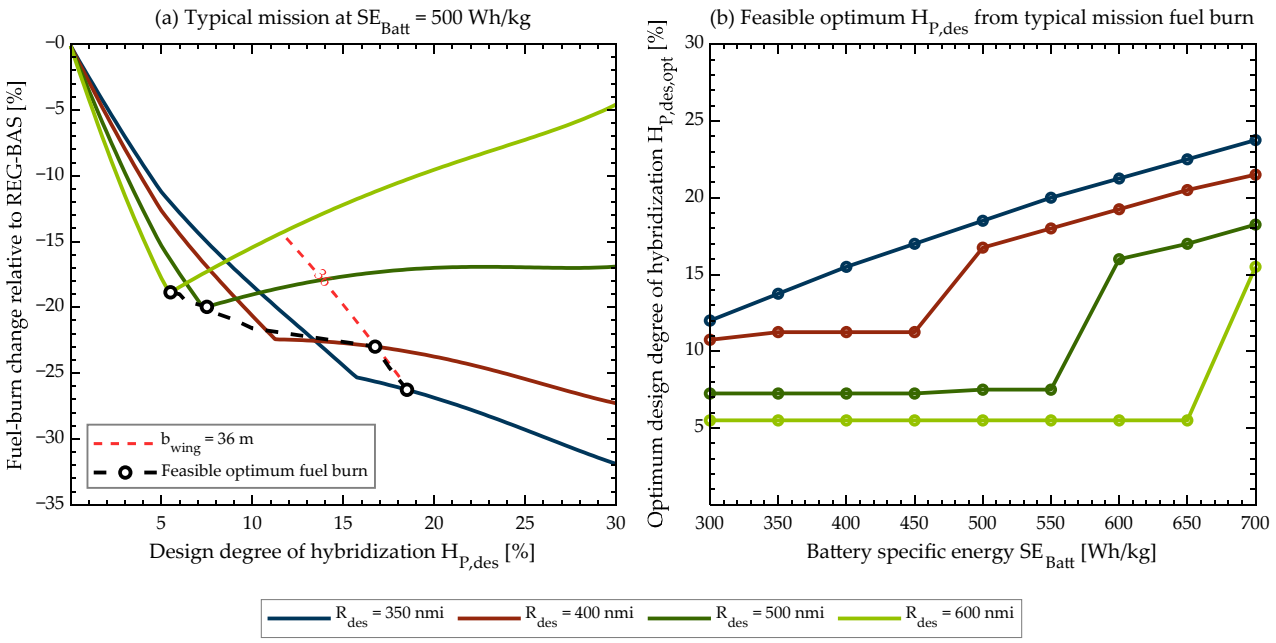


Figure 12. Design range sensitivity of newly sized regional hybrid electric aircraft on typical mission performance: (**a**) relative block fuel for varying design degrees of hybridization at 500 Wh/kg and (**b**) resulting optimum design degree of hybridization over battery specific energy.

Another effect can be observed for smaller design mission ranges. Here, further increases in design hybridization continue to improve the typical mission fuel burn, even beyond the point where the maximum hybridization limit is reached. Although part of the installed battery capacity remains unused, the additional improvements in propulsion system efficiency can still overcompensate the associated HEP mass penalty. This aligns with the trends previously observed for higher battery specific energies (see Figure 8b).

For larger design ranges, the optimum typical mission fuel burn is reached at the kink point, where the installed battery capacity is fully utilized while simultaneously reaching $H_{P,max}$. For shorter design ranges, however, a shift in the optimum HEP sizing point can be seen. In these cases, the optimum design point jumps away from the kink point towards the ICAO code C wing span constraint (see Figure 12a). Overall, the optimum typical mission fuel burn delta reduces moderately from −23% to −19%, when increasing the design range from 400 nmi to 600 nmi.

For each combination of design range and battery specific energy, the design degree of hybridization that minimizes typical mission fuel burn is obtained. The resulting optimum hybridization degree $H_{P,des,opt}$ is shown in Figure 12b over the battery specific energy, which is varied between 300 and 700 Wh/kg. For a specific energy of 500 Wh/kg, the optimum design points match those identified in Figure 12a. Overall, longer design ranges shift the optimum towards lower values of $H_{P,des,opt}$, whereas decreasing the design range results in larger HEP sizes. This trend reflects the aircraft-level effects discussed previously. Furthermore, improving the battery technology generally moves the fuel burn optimum towards higher hybridization degrees, as the reduced battery mass impact allows a larger amount of electrical energy to be installed.

Additionally, the previously discussed step changes in $H_{P,des,opt}$ are clearly visible in Figure 12b as sudden jumps in the optimum hybridization degree with increasing design range. They correspond to the shift of the optimum sizing point from the hybridization limit (kink point) towards the geometric wing span constraint. With increasing design range, this transition occurs at higher battery specific energies, as more advanced battery technologies are required before larger HEP sizes become more beneficial.

In the next step, the aircraft mission performance is evaluated at the previously determined optimum hybridization degree $H_{P,des,opt}$ (see Figure 12b). The resulting relative fuel burn compared with the baseline over the battery specific energy is displayed in Figure 13 for both the design mission (a) and the typical mission (b).

As described above, the HEP is sized to minimize fuel burn on the typical mission, even if this results in a worse fuel burn performance on the design mission. As expected, increasing the design range reduces the achievable fuel burn benefit on both missions. At lower battery specific energies, the mission performance is relatively similar across all design ranges. As battery technology improves, however, the fuel burn trends show a stronger divergence between the design ranges. This indicates that larger aircraft continue to be affected by a stronger mass penalty, even when advanced battery technologies are assumed. Furthermore, increasing the design range makes it more difficult to overcome the kink point as the optimum sizing point (see Figure 12).

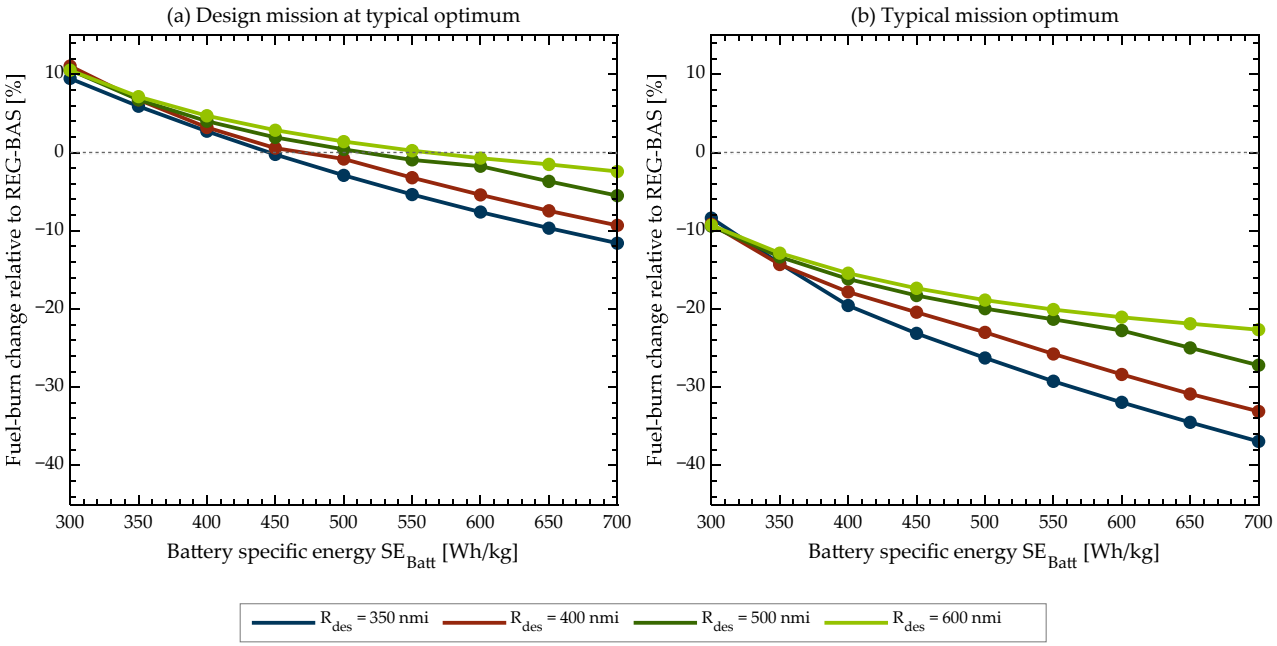


Figure 13. Design range sensitivity of regional hybrid electric aircraft mission performance: relative block fuel over battery specific energy for (**a**) the design mission and (**b**) the typical mission (Note: each aircraft is sized at its typical mission optimum design degree of hybridization).

Another overall trend visible in Figure 13 is the positive impact of battery technology on overall mission performance. For battery specific energies below 450 Wh/kg, all investigated aircraft configurations show a higher design mission fuel burn than the baseline aircraft. Even for the worst battery technologies assumed, the design mission fuel burn penalty stays within around 10%. A trend reversal can be observed between 450 and 550 Wh/kg, where the design mission penalty decreases and fuel burn improvements become achievable. At 500 Wh/kg, the aircraft with the largest design range of 600 nmi still performs only around 2% worse than the baseline aircraft. For battery technologies beyond 550 Wh/kg, all investigated aircraft achieve fuel burn reductions for the design mission.

For the typical mission, substantial fuel burn benefits are achieved across all design ranges and battery technologies. At the lowest battery specific energy of 300 Wh/kg, all aircraft reduce typical fuel burn by around 10%. At 500 Wh/kg, the aircraft with the largest design range (600 nmi) still achieves a fuel burn reduction of around 19%. For the smallest aircraft (350 nmi), a reduction of approximately 26% is reached. With further

improvements in battery technology, typical fuel burn improvements beyond 30% become achievable for smaller regional aircraft configurations.

An overview of the design and typical mission performance at different design ranges and battery technologies is provided in Figure A3. Additionally, Figure A4 displays the key aircraft parameters if the HEP system is optimized for the design mission (a) or the typical mission (b).

5. Discussion

A general statement on the potential of parallel hybrid electric or electrically assisted propulsion systems is less straightforward than might initially be assumed. It is already well established from the literature (e.g., [5,11,22,26]) that the underlying battery technology has a decisive influence on the overall mission fuel burn of such systems. Similar to the results presented in [9,25], it was shown in this paper that at a battery system specific energy of around 500 Wh/kg, design mission fuel burn benefits are achievable for the regional application. Based on recent battery research, this technology leap could be achievable by the end of the following decade [7,8].

Nevertheless, the influence of the mission distance is often underestimated or neglected, despite having a similar or even larger impact on the overall aircraft performance. Since the battery is sized for the design mission, the hybridization degree can be increased during shorter, typically flown missions. As a result, substantial mission block fuel improvements are obtained for both aircraft applications. Consequently, the sizing of the HEP components should not be based exclusively on the design mission. Instead, it can be tailored to achieve a best-and-balanced aircraft performance on both missions. Thus, to assess the overall potential of parallel HEP systems, the actual aircraft utilization becomes especially relevant [83].

Besides the previously mentioned aspects, the selected aircraft category plays a major role in the performance evaluation. In contrast to retrofit approaches [14,84], this study considers the sizing of both baseline and hybrid aircraft for identical payload–range requirements. While the regional aircraft showed a relatively small impact on design mission fuel burn with increasing battery size, the helicopter mission performance was significantly more sensitive to additional HEP component masses, mostly due to the larger OEM share of the helicopter. Hence, the investigated propulsion concept seems less beneficial for use in medium-sized helicopters than for regional aircraft.

On the propulsion system level, the partial electrification of the compressor system has implications on the operability of the engine and its allowable hybridization range [15]. Many previous studies assumed a reduction in gas turbine size with increased design hybridization (e.g., [11,22,27]). However, to avoid engine shutdown in case of electric system failure, specific mitigation measures, including gas turbine oversizing, had to be incorporated into the models. Despite the negative impact on propulsion system mass and efficiency, the results of this study showed that oversizing increases the operational hybridization range and enables operation without electrical assistance. Compared with previous studies, this avoids the need to size the battery system for additional electrification during contingencies and reserves.

At the aircraft level, additional geometric constraints, such as the ICAO code C wing span limitation, may become active with increasing battery size, thus limiting the overall hybridization potential. To alleviate this, adaptations in wing loading, aspect ratio or even more futuristic wing designs, such as foldable wing tips or box-wing configurations, might be considered [38]. With increasing design range, the wing span constraint becomes less relevant, as the optimum degree of hybridization and corresponding fuel burn benefit decrease. Despite this, the investigated propulsion concept still achieves meaningful

typical mission fuel burn reductions, demonstrating its scalability towards larger regional aircraft.

In this paper, mission block fuel was used as the key metric for the aircraft-level investigations of the HybVer propulsion system concept. When expanding this assessment towards a climate impact analysis, non-CO_2 emissions such as NO_x, as well as the upstream pathways for both electricity and fuel production, need to be considered. Despite the improvements in typical mission fuel burn, both investigated hybrid electric applications show a higher total in-flight energy consumption (fuel + electricity) relative to the baseline case. However, for the evaluation of overall climate impact, a well-to-wake analysis would be required, especially if Sustainable Aviation Fuels (SAF) are considered. Regarding NO_x emissions, the proposed electrically assisted propulsion system may be beneficial in two ways: First, the partial electric drive of the compressor lowers the combustion temperatures (e.g., T_4) during normal operation. Second, the applied oversizing measures further reduce the operating temperatures. Both effects are expected to have a positive impact on NO_x emissions when compared with a baseline aircraft without electrical assistance [85].

Although the present study makes significant progress regarding the four common limitations identified from previous studies, several opportunities for further improvement exist. They can be grouped into three categories: selected technology and application assumptions, methodological limitations and the scope of the study. First, uncertainties in the underlying assumptions include the selected Y2035+ technology levels, the specific power and efficiencies of the electrical components or the selection of the helicopter's typical mission range based on limited available data. Second, the methodological simplifications include the regional structural mass estimation, the neglect of geometric changes on nacelle drag, the high-level battery sizing and performance model, the thermal management design, the regional mission calculation, the constant hybridization strategy or the limited number of helicopter validation cases. Third, the scope of the present study is limited to the cycle-integrated parallel hybrid configuration (e.g., excluding multi-motor or DEP architectures) and does not include any payload–range analyses or sensitivities of additional technology assumptions. Among these aspects, two key limitations are especially impactful on the overall results: the current modeling of the regional mission as well as the simplified battery model.

Currently, the mission calculation of the regional aircraft is conducted based on a typical mid-cruise point only. Other mission segments, such as climb, take-off or descent, are not explicitly modeled, which prevents further analysis such as segment-based hybridization strategies. Even though the LTO fuel was considered through a constant MTOM fraction, a more detailed calculation would refine the mission performance results. This is especially relevant for shorter mission ranges, where the LTO fuel takes up a larger share of the total mission [86].

In addition, the current battery modeling only considers the available usable energy content at the system level. As many studies state battery specific energy at the cell level, a more detailed consideration of cell-to-system effects would improve the overall comparability. Furthermore, battery aging effects or limitations of the discharge rate were not taken into account in the presented models. With increasing battery age, the discharge efficiency and usable energy capacity decline, reducing the achievable hybridization degree as well as the mission fuel burn benefits over time. Similarly, a limitation of the discharge rate could restrict how much the installed battery capacity can be utilized over the mission. This might potentially limit the operational hybridization degree and the achievable fuel burn benefit, especially on shorter missions [34]. Building upon the identified limitations, specific suggestions for future improvements are provided in Section 6.2.

6. Conclusions and Outlook

6.1. Key Findings

An integrated methodology combining the sizing and performance evaluation of a parallel hybrid electric propulsion system at the aircraft level has been introduced. The methodology was applied to a CIPH concept, in which electrical power sourced from an on-board battery system is supplied to the compressor system in two ways: first, by directly assisting the HP shaft and second, by driving the outer rotors of a counter-rotating compressor.

The propulsion system was investigated for two aircraft categories: a regional aircraft (50 PAX) and a medium-sized helicopter (19 PAX). For both applications, technology projections for the aircraft and HEP components were applied for an EIS in Y2035+. The study focused especially on the operational limitations of the propulsion systems, the use of oversizing and other mitigation measures to account for electric system failure and the resulting effects on battery sizing, aircraft design and mission performance.

At the propulsion system level, it was found that increasing electrical assistance significantly improves overall propulsion system efficiency. At the same time, the required oversizing measures negatively affect the gas turbine mass and thermodynamic cycle. However, they not only ensure safe operation without electrical assistance, but also enable higher maximum hybridization degrees, which can be exploited during off-design missions.

At the aircraft level, parametric investigations were performed for different hybridization levels and battery technologies. Besides the assumed battery specific energy, the evaluated mission range was identified as a key parameter affecting the overall results.

For the regional application, a design degree of hybridization of $H_{P,des}$ = 11% was selected at a battery system specific energy of 500 Wh/kg. On the design mission, the resulting battery mass largely counteracts the SFC improvements, resulting in only minor fuel burn improvements. However, on the typical mission, a block fuel reduction of 22% is achieved. For the shorter mission, the installed battery capacity can be fully utilized, increasing the off-design degree of hybridization to $H_{P,typ}$ = 34%. Without the ICAO code C wing span constraint, even higher typical mission fuel burn reductions would be possible.

The helicopter application was more sensitive to HEP mass increases and showed a smaller difference between design and typical mission range. In addition, the oversizing measures led to a larger penalty in propulsion system efficiency. This resulted in an increase in design mission block fuel by 11%, at a prescribed design degree of hybridization of $H_{P,des}$ = 8%. Nevertheless, the shorter typical mission still benefits from increased hybridization degrees, reaching $H_{P,typ}$ = 18% and reducing typical mission fuel burn by 10%.

The design range sensitivity study showed that increasing aircraft size and range will reduce both the optimum degree of hybridization and the achievable fuel burn benefit. Nevertheless, even for a design range of 600 nmi, the investigated propulsion concept still achieved a typical mission fuel burn reduction of 19%, indicating good scalability towards larger regional applications.

Overall, the results show that the most beneficial propulsion system sizing is not necessarily determined by the design mission alone, but by how the aircraft is actually operated. As most aircraft are flown well below their design range, fully utilizing the installed battery capacity on these shorter missions greatly reduces mission fuel burn.

The presented results were put into perspective and interpreted at the aircraft level, with key assumptions and limitations of the study being identified. These limitations can be grouped into three categories, namely technology and application assumptions, methodological limitations and the overall scope of the study. Among the underlying technology assumptions, the efficiency and specific power of the HEP components were most

impactful on the overall results. Regarding the methodological limitations, future work could refine the performance, thermal and mass modeling of the battery system as well as the simplified regional mission calculation. To address these, further improvements and extensions of the methodology will be suggested in the next section.

6.2. Further Work

Based on the findings and limitations of the present study, further research and development should be conducted. The presented methodology establishes a foundation for the coupled assessment of hybrid electric propulsion systems at the aircraft level and can be applied to other parallel HEP architectures (e.g., multi-motor configurations, MIPH systems or discrete parallel hybrid systems). It could be further extended to accommodate hydrogen-powered aircraft configurations, enabling the evaluation of fuel cell-assisted propulsion concepts. Besides this, further aircraft classes could be examined to assess the overall scalability of the investigated propulsion concepts.

Further extensions of the methodology could include higher-fidelity battery models at the cell level. One improvement would be the inclusion of minimum and maximum state-of-charge limits to account for battery life degradation. This would influence the overall battery sizing, as the usable depth of discharge is reduced. In addition, a maximum discharge rate could be included in the models, potentially limiting the battery utilization during short off-design missions. Integrating battery discharge efficiency curves would further improve the overall accuracy of the models.

For the regional aircraft application, the mission calculation could be refined by implementing a segment-based approach. This would enable the evaluation of the propulsion system behavior and battery utilization over the flight mission, hence enabling the investigation of different hybridization strategies to further improve aircraft performance. Another improvement would be a more refined calculation of the LTO fuel and the consideration of electric taxiing, as the impact on mission block fuel becomes especially relevant during small mission ranges.

At the aircraft level, more detailed investigations into other off-design missions (besides the typical mission) could be performed. Of interest would be the trend of key performance parameters (e.g., battery utilization, hybridization degree, mission block fuel) over different flight ranges, under consideration of inherent operational constraints. Furthermore, the visualization of these parameters over the entire payload–range profile of the hybrid electric aircraft would provide additional insights.

Beyond the aircraft level, perhaps the most essential extension of the presented methodology is the integration of representative fleet operation. While the current study solely focuses on the design and typical mission analysis, the overall potential of electrically assisted HEP systems can only be assessed by including actual aircraft utilization derived from flight data. Further work should hence incorporate realistic mission range distributions to enable fleet-level optimization of the HEP system sizing. This would allow future propulsion systems to be tailored to its actual operational usage rather than a single mission.

Author Contributions: Conceptualization, P.M., A.S. and M.H.; methodology, P.M., C.W. and A.S.; software, P.M., C.W. and A.S.; validation, P.M. and A.S.; formal analysis, P.M. and C.W.; investigation, P.M., C.W. and A.S.; resources, M.H.; data curation, P.M., C.W. and A.S.; writing—original draft preparation, P.M. and A.S.; writing—review and editing, P.M., C.W., A.S. and M.H.; visualization, P.M.; supervision, A.S. and M.H.; project administration, P.M. and A.S.; funding acquisition, P.M., A.S. and M.H. All authors have read and agreed to the published version of the manuscript.

Funding: This research was funded by the BMWK (Federal Ministry for Economic Affairs and Climate Action of Germany) through Luftfahrtforschungsprogramm-VI-2 (Grant number: 20E2111A).

https://doi.org/10.3390/aerospace13111010

Data Availability Statement: The original contributions presented in this study are included in this article. Further inquiries should be directed to the corresponding author.

Acknowledgments: The authors would like to thank our colleagues Moritz G. Kolb and Raoul Böck for their continuous support and the fruitful discussions. In addition, we gratefully acknowledge Federico Tamayo Peinado for his exceptional support on the rotorcraft modeling. We especially thank Reinhold Schaber from MTU Aero Engines AG and Bernd Becker from Rolls-Royce Deutschland Ltd. & Co KG for their ongoing interest and valuable feedback. We would also like to thank Fabian Peter for the constructive review and feedback on the manuscript. Lastly, we would personally thank Jan Nittka, Lucas Schreer and Yinghui Yang for their valuable collaboration, constructive discussions and support throughout the HybVer project.

Conflicts of Interest: The authors declare no conflicts of interest. The funders had no role in the design of the study; in the collection, analyses, or interpretation of data; in the writing of the manuscript; or in the decision to publish the results.

Abbreviations

The following abbreviations are used in this manuscript:

APSS	Aircraft Propulsion System Simulation
BAS	BASeline
BLADE	Bauhaus Luftfahrt Aircraft Design Environment
BLI	Boundary Layer Ingestion
CIPH	Cycle-Integrated Parallel Hybrid
CRC	Counter-Rotating Compressor
DoD	Depth of Discharge
DL	Disc Loading
EPFA	Equivalent Flat Plate Area
EIS	Entry-Into-Service
FL	Flight Level
GBX	GearBox
GT	Gas Turbine
HEL	HELicopter
HEL-BAS	HELicopter-BASeline
HEL-HYB	HELicopter-HYBrid
HEL-REF	HELicopter-REFerence
HEP	Hybrid-Electric Propulsion
IGE	In-Ground-Effect
IGW	Instantaneous Gross Weight
ISA	International Standard Atmosphere
HOGE	Hover Out of Ground Effect
HOVER	HelicOpter design and performance eValuation framEwoRk
HP	High Pressure
HPC	High Pressure Compressor
HPT	High Pressure Turbine
HYB	HYBrid electric
HybVer	Hybridisierte Verdichterkonzepte (Hybridized Compressor Concepts)
ICAO	International Civil Aviation Organization
IMOTHEP	Investigation and Maturation of Technologies for Hybrid-Electric Propulsion
L/D	Lift-to-Drag
LPC	Low Pressure Compressor
LPT	Low Pressure Turbine
LTO	Landing Take-Off
MATLAB	MATrix LABoratories
MIPH	Mechanically Integrated Parallel Hybrid
MTOM	Maximum Take-Off Mass
OAG	Oil-And-Gas

OEM	Operational Empty Mass
OPR	Overall Pressure Ratio
PAX	Passengers
PMAD	Power Management And Distribution
PMSM	Permanent Magnet Synchronous Machine
PSFC	Power-Specific Fuel Consumption
REG	REGional
REG-BAS	REGional-BASeline
REG-HYB	REGional-HYBrid
REG-REF	REGional-REFerence
REF	REFerence
SAF	Sustainable Aviation Fuel
SAR	Search-And-Rescue
SAS	Simplified Aircraft Scaling
SLS	Sea Level Static
SM	Surge Margin
SUAVE	Stanford University Aerospace Vehicle Environment
TLAR	Top-Level Aircraft Requirements
TMS	Thermal Management System
TOM	Take-Off Mass
TSFC	Thrust-Specific Fuel Consumption

Appendix A

Appendix A.1. Propulsion System Oversizing Measures

Table A1. Applied gas turbine oversizing parameters for the REG-HYB configuration and their impact on cruise PSFC and GT mass relative to the REG-BAS.

Parameter	Unit	REG-BAS	REG-HYB ($H_{P,des}$ = 30%)			
			Without Oversizing	Delta (%)	With Oversizing	Delta (%)
$T_{4,cr}$	K	1569	1569	0%	1095	−30%
Rel. bleed air LPC	-	0	0	-	0.18	-
Beta LPC	-	0.5	0.5	-	0.4	−20%
Beta HPC	-	0.6	0.6	-	0.3	−50%
$PSFC_{cr}$	kg/kWh	0.29	0.17	−40%	0.16	−45%
GT mass	kg	453	172	−62%	551	22%

https://doi.org/10.3390/aerospace13111010

Appendix A.2. Aircraft Energy Consumption

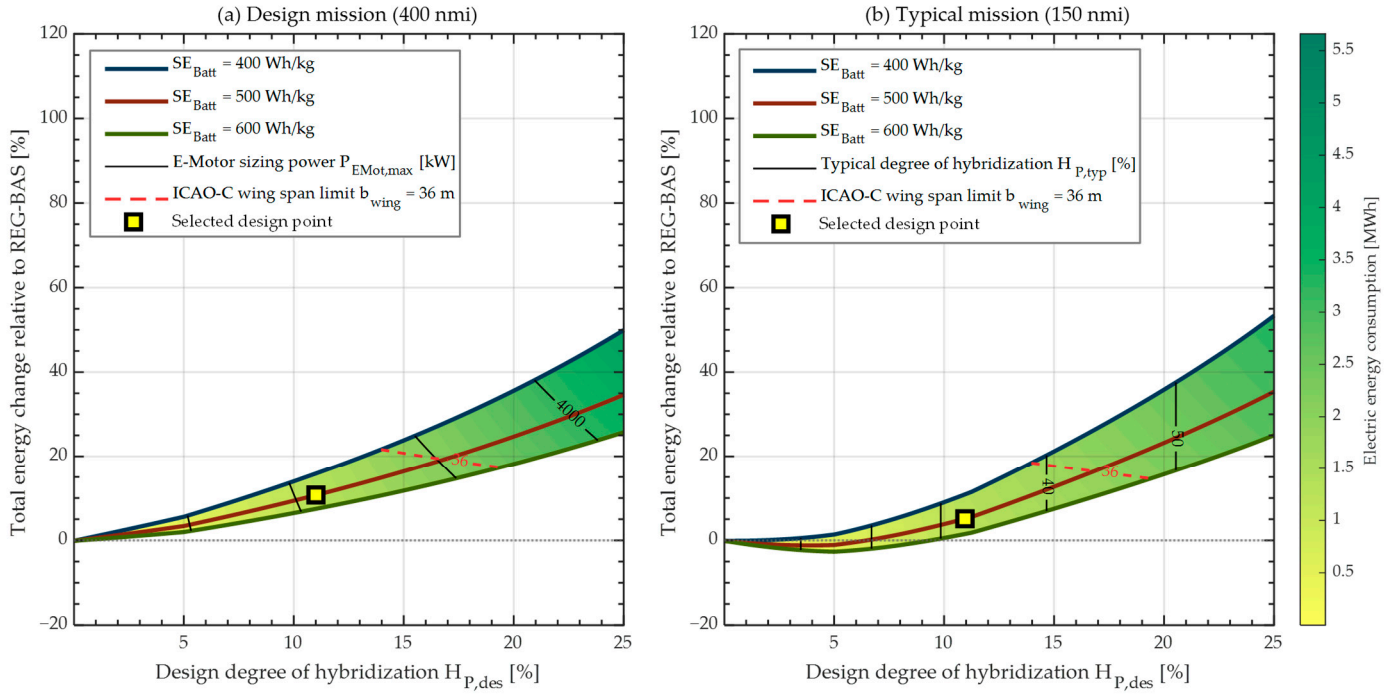


Figure A1. Regional hybrid electric aircraft relative block energy for (**a**) the design mission and (**b**) the typical mission, with varying design degrees of hybridization and battery technologies.

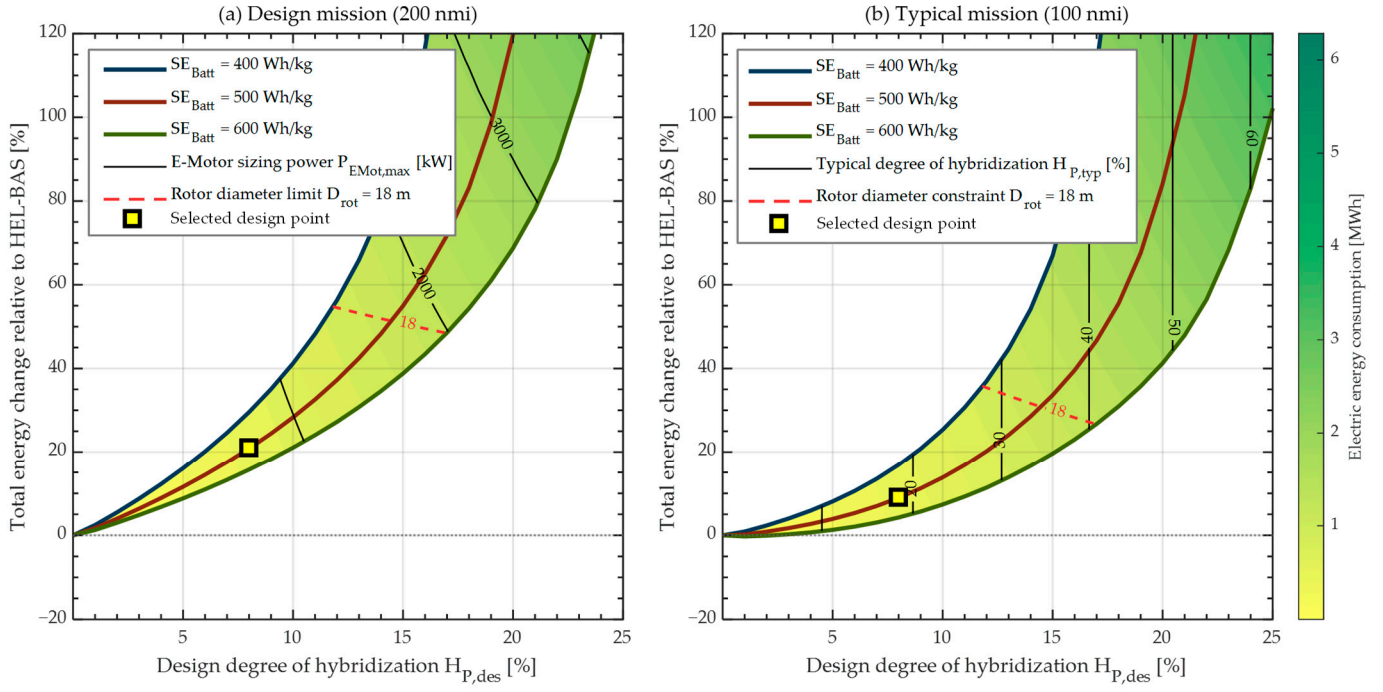


Figure A2. Hybrid electric helicopter relative block energy for (**a**) the design mission and (**b**) the typical mission, with varying design degrees of hybridization and battery technologies.

https://doi.org/10.3390/aerospace13111010

Appendix A.3. Regional Aircraft Design Range Sensitivity Results

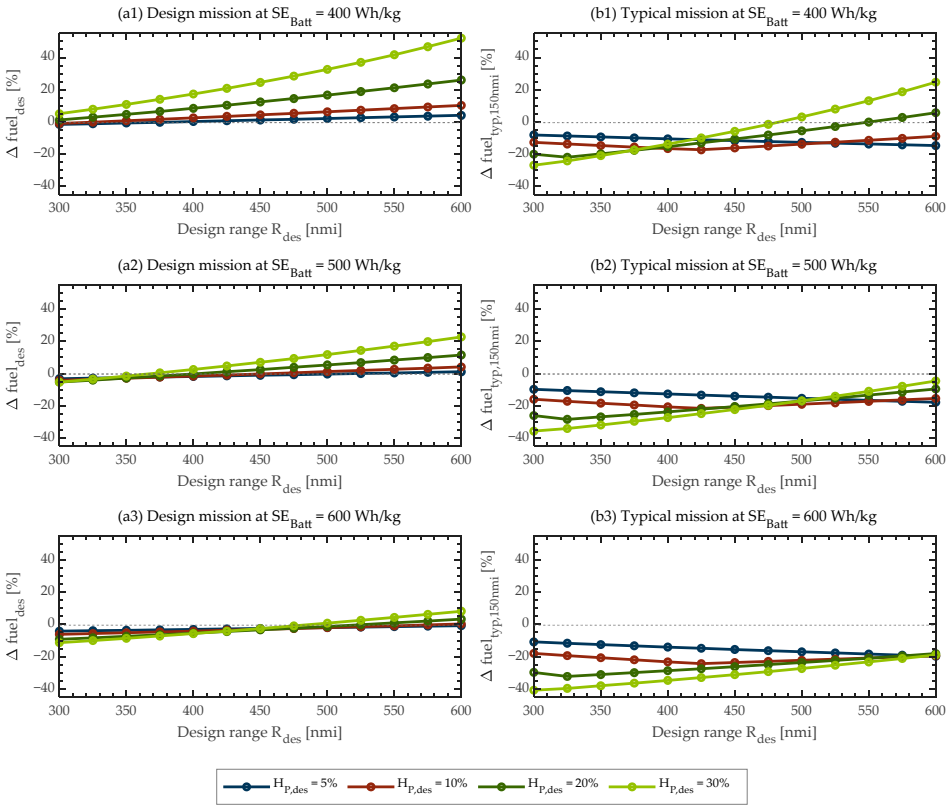


Figure A3. Design range sensitivity on (**a1–a3**) design and (**b1–b3**) typical mission for varying $H_{P,des}$ and SE_{Batt}.

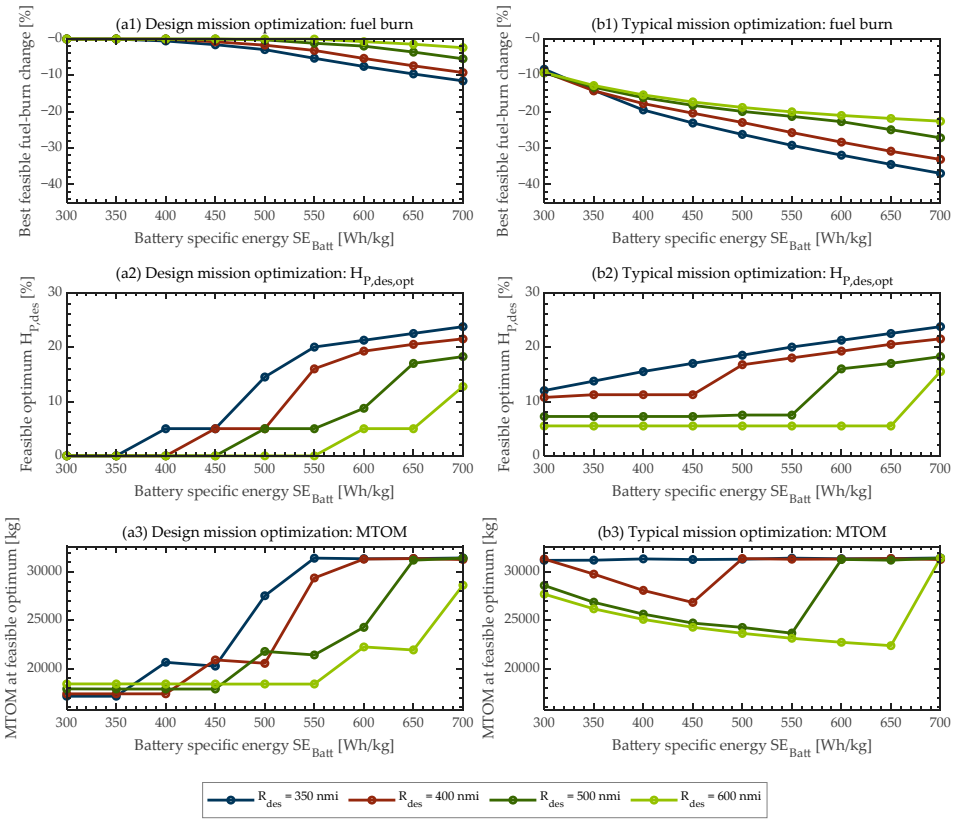


Figure A4. Design range sensitivity on aircraft results at (**a1–a3**) design and (**b1–b3**) typical mission optimum.

https://doi.org/10.3390/aerospace13111010

References

1. Pornet, C.; Isikveren, A.T. Conceptual design of hybrid-electric transport aircraft. *Prog. Aerosp. Sci.* **2015**, *79*, 114–135. https://doi.org/10.1016/j.paerosci.2015.09.002.
2. Schmitz, O.; Hornung, M. Unified Applicable Propulsion System Performance Metrics. *J. Eng. Gas Turbines Power* **2013**, *135*, 111201. https://doi.org/10.1115/1.4025066.
3. Isikveren, A.T.; Kaiser, S.; Pornet, C.; Vratny, P.C. Pre-design strategies and sizing techniques for dual-energy aircraft. *Aircr. Eng. Aerosp. Technol. J.* **2014**, *86*, 525–542. https://doi.org/10.1108/AEAT-08-2014-0122.
4. Lorenz, L.; Seitz, A.; Kuhn, H.; Sizmann, A. Hybrid Power Trains for Future Mobility. In *Proceedings of the 62. Deutscher Luft- und Raumfahrtkongress (DLRK), Stuttgart, Germany, 10–12 September* 2013; DGLR (Deutsche Gesellschaft für Luft- und Raumfahrt), Ed.; Deutsche Gesellschaft für Luft- und Raumfahrt—Lilienthal-Oberth e.V.: Bonn, Germany, 2013.
5. Pornet, C.; Gologan, C.; Vratny, P.C.; Seitz, A.; Schmitz, O.; Isikveren, A.T.; Hornung, M. Methodology for Sizing and Performance Assessment of Hybrid Energy Aircraft. *J. Aircr.* **2015**, *52*, 341–352. https://doi.org/10.2514/1.C032716.
6. Zamboni, J.; Vos, R.; Emeneth, M.; Schneegans, A. A Method for the Conceptual Design of Hybrid Electric Aircraft. In *AIAA Scitech 2019 Forum*; AIAA Scitech 2019 Forum, San Diego, California; American Institute of Aeronautics and Astronautics: Reston, Virginia, 2019; ISBN 978-1-62410-578-4.
7. Kühnelt, H.; Mastropierro, F.; Zhang, N.; Toghyani, S.; Krewer, U. Are batteries fit for hybrid-electric regional aircraft? *J. Phys. Conf. Ser.* **2023**, *2526*, 12026. https://doi.org/10.1088/1742-6596/2526/1/012026.
8. Pattanayak, T.; Mavris, D. Battery technology for sustainable aviation: A review of current trends and future prospects. *Appl. Energy* **2025**, *397*, 126356. https://doi.org/10.1016/j.apenergy.2025.126356.
9. Palaia, G.; Abu Salem, K.; Quarta, A.A. Parametric Analysis for Hybrid–Electric Regional Aircraft Conceptual Design and Development. *Appl. Sci.* **2023**, *13*, 11113. https://doi.org/10.3390/app131911113.
10. Bills, A.; Sripad, S.; Fredericks, W.L.; Singh, M.; Viswanathan, V. Performance Metrics Required of Next-Generation Batteries to Electrify Commercial Aircraft. *ACS Energy Lett.* **2020**, *5*, 663–668. https://doi.org/10.1021/acsenergylett.9b02574.
11. Antcliff, K.R.; Guynn, M.D.; Marien, T.; Wells, D.P.; Schneider, S.J.; Tong, M.J. Mission Analysis and Aircraft Sizing of a Hybrid-Electric Regional Aircraft. In *Proceedings of the 54th AIAA Aerospace Sciences Meeting 2016, San Diego, CA, USA, 4–8 January 2016*; Curran Associates Inc: Red Hook, NY, USA, 2016; pp 1–16, ISBN 978-1-62410-393-3.
12. Seitz, A.; Nickl, M.; Stroh, A.; Vratny, P.C. Conceptual study of a mechanically integrated parallel hybrid electric turbofan. *Proc. Inst. Mech. Eng. Part G J. Aerosp. Eng.* **2018**, *232*, 2688–2712. https://doi.org/10.1177/0954410018790141.
13. Vries, R.d.; Brown, M.; Vos, R. Preliminary Sizing Method for Hybrid-Electric Distributed-Propulsion Aircraft. *J. Aircr.* **2019**, *56*, 2172–2188. https://doi.org/10.2514/1.C035388.
14. Vratny, P.C.; Kaiser, S.; Seitz, A.; Donnerhack, S. Performance Investigation of Cycle-Integrated Parallel Hybrid Turboshafts. *J. Eng. Gas Turbines Power* **2017**, *139*, 31201. https://doi.org/10.1115/1.4034498.
15. Maas, P.; Warsch, C.; Böck, R.; Kolb, M.G.; Seitz, A. Pre-Design Investigation of a Propulsion System with Compressor Electric Drive. In *Proceedings of the 73. Deutscher Luft- und Raumfahrtkongress (DLRK), Hamburg, Germany, 30 September–2 October* 2024; DGLR (Deutsche Gesellschaft für Luft- und Raumfahrt), Ed.; Deutsche Gesellschaft für Luft- und Raumfahrt—Lilienthal-Oberth e.V.: Bonn, Germany, 2024.
16. Maas, P.; Seitz, A.; Wirth, D.; Geiger, P.; Hornung, M. Performance Investigations of a Cycle- and Mechanically-Integrated Parallel Hybrid-Electric Turboshaft. In *Proceedings of the 12th EASN International Conference, Barcelona, Spain, 8–11 October 2022*; EASN (The European Aeronautics Science Network), Ed.; EASN (The European Aeronautics Science Network): Brussels, Belgium, 2022; https://doi.org/10.5281/zenodo.7785239.
17. van Holsteijn, M.R.; Gangoli Rao, A.; Yin, F. Operating Characteristics of an Electrically Assisted Turbofan Engine. In *Proceedings of the ASME Turbo Expo 2020: Turbomachinery Technical Conference and Exposition—2020, Presented at the ASME Turbo Expo 2020: Turbomachinery Technical Conference and Exposition, online, 21-25 September 2020*; The American Society of Mechanical Engineers; Curran Associates Inc: New York, NY, USA, Red Hook, NY,USA, 2020; ISBN 978-0-7918-8405-8.
18. Kang, S.; Roumeliotis, I.; Zhang, J.; Broca, O.; Pachidis, V. Assessment of Engine Operability and Overall Performance for Parallel Hybrid Electric Propulsion Systems for a Single-Aisle Aircraft. *J. Eng. Gas Turbines Power* **2022**, *144*, 041002. https://doi.org/10.1115/1.4052880.
19. Chapman, J.W. A Study of Large Scale Power Extraction and Insertion on Turbofan Performance and Stability. In *AIAA Propulsion and Energy 2020 Forum*; VIRTUAL EVENT: Reston, Virginia, 2020; ISBN 978-1-62410-602-6.
20. Bijewitz, J.; Seitz, A.; Hornung, M. Power Plant Pre-Design Exploration for a Turbo-Electric Propulsive Fuselage Concept. In *Proceedings of the Joint Propulsion Conference, 2018 Joint Propulsion Conference, Cincinnati, Ohio, 9–11 July 2018*; AIAA (The

American Institute of Aeronautics and Astronautics), Ed.; AIAA (The American Institute of Aeronautics and Astronautics): Reston, Virginia, 2018; ISBN 978-1-62410-570-8.
21. Nittka, J.; Peitsch, D. Operability Implications of Speed Variability in Hybridised Vaneless Counter-Rotating Axial Compressor Concepts. *Aerospace* **2026**, *13*, 304. https://doi.org/10.3390/aerospace13040304.
22. Voskuijl, M.; van Bogaert, J.; Rao, A.G. Analysis and design of hybrid electric regional turboprop aircraft. *CEAS Aeronaut. J.* **2018**, *9*, 15–25. https://doi.org/10.1007/s13272-017-0272-1.
23. Hoelzen, J.; Liu, Y.; Bensmann, B.; Winnefeld, C.; Elham, A.; Friedrichs, J.; Hanke-Rauschenbach, R. Conceptual Design of Operation Strategies for Hybrid Electric Aircraft. *Energies* **2018**, *11*, 217. https://doi.org/10.3390/en11010217.
24. Orefice, F.; Marciello, V.; Cusati, V.; Nicolosi, F. Powertrain Model Improvement for Hybrid-Electric Regional Aircraft. In *AIAA SCITECH 2022 Forum*, San Diego, CA & Virtual; Reston, Virginia, 2022; ISBN 978-1-62410-631-6.
25. Marciello, V.; Di Stasio, M.; Ruocco, M.; Trifari, V.; Nicolosi, F.; Meindl, M.; Lemoine, B.; Caliandro, P. Design Exploration for Sustainable Regional Hybrid-Electric Aircraft: A Study Based on Technology Forecasts. *Aerospace* **2023**, *10*, 165. https://doi.org/10.3390/aerospace10020165.
26. Habermann, A.L.; Kolb, M.G.; Maas, P.; Kellermann, H.; Rischmüller, C.; Peter, F.; Seitz, A. Study of a Regional Turboprop Aircraft with Electrically Assisted Turboshaft. *Aerospace* **2023**, *10*, 529. https://doi.org/10.3390/aerospace10060529.
27. Ang, A.W.X.; Gangoli Rao, A.; Kanakis, T.; Lammen, W. Performance analysis of an electrically assisted propulsion system for a short-range civil aircraft. *Proc. Inst. Mech. Eng. Part G J. Aerosp. Eng.* **2019**, *233*, 1490–1502. https://doi.org/10.1177/0954410017754146.
28. Pham, D.D.-T.V.; Naik, A.M.; Recine, C.J.; Joseph, J.; Listgarten, N.S.; Natividad, C.A.D.; Park, J.; Wishart, J.M. Performance Scaling of Multi-Class Parallel Hybrid-Electric Regional Turboprop Airliner Concepts. In *Proceedings of the 2025 IEEE/AIAA Transportation Electrification Conference and Electric Aircraft Technologies Symposium (ITEC+EATS), Anaheim, CA, USA, 18–20 June 2025*; IEEE: New York, NY, USA, 2025; pp 1–6, ISBN 979-8-3315-2214-8.
29. Shamiyeh, M. Conceptual Design of a Hybrid Electric Rotorcraft. Master Thesis, TUM (Technische Universität München), Munich, Germany, 2015.
30. Saias, C.A.; Goulos, I.; Roumeliotis, I.; Pachidis, V.; Bacic, M. Preliminary Design of Hybrid-Electric Propulsion Systems for Emerging Urban Air Mobility Rotorcraft Architectures. *J. Eng. Gas Turbines Power* **2021**, *143*, 041002. https://doi.org/10.1115/1.4052057.
31. Roumeliotis, I.; Arena, F.; Liu, Y.; Vouros, S.; Pachidis, V.; Broca, O.; Toure, D.; Unlu, D. Performance and Emission Assessment of Thermo-Electric Power Plant for Rotorcraft Propulsion. In *Proceedings of the ASME Turbo Expo 2020: Turbomachinery Technical Conference and Exposition, Virtual, Online*; *Volume 5: Controls, Diagnostics, and Instrumentation; Cycle Innovations; Cycle Innovations: Energy Storage*; American Society of Mechanical Engineers: New York, NY, USA, 2020; ISBN 978-0-7918-8414-0.
32. Kang, S.; Saias, C.A.; Roumeliotis, I.; Broca, O. Preliminary Design of Integrated Power and Thermal Management Systems for Hybrid Electric VTOL Aircraft Architecture. In *Proceedings of the ASME Turbo Expo 2025: Turbomachinery Technical Conference and Exposition, Memphis, TE, USA, 16–20 June 2025*; *Volume 4: Controls, Diagnostics & Instrumentation; Cycle Innovations; Education; Electric Power*; American Society of Mechanical Engineers: New York, NY, USA, 2025; ISBN 978-0-7918-8880-3.
33. Saias, C.A.; Roumeliotis, I.; Goulos, I.; Pachidis, V.; Bacic, M. Design Exploration and Performance Assessment of Advanced Recuperated Hybrid-Electric Urban Air Mobility Rotorcraft. *J. Eng. Gas Turbines Power* **2022**, *144*, 031023. https://doi.org/10.1115/1.4052955.
34. Bonnin, V.O.; Hoogreef, M.F.M. Exploration of Off-Design Performance for Hybrid Electric Regional Aircraft. *J. Aircr.* **2025**, *62*, 876–895. https://doi.org/10.2514/1.C037893.
35. Quillet, D.; Boulanger, V.; Rancourt, D. Off-Design Performance Analysis of a Parallel Hybrid Electric Regional Turboprop Aircraft. *J. Aircr.* **2023**, *60*, 1728–1738. https://doi.org/10.2514/1.C036927.
36. Palaia, G.; Abu Salem, K. Mission Performance Analysis of Hybrid-Electric Regional Aircraft. *Aerospace* **2023**, *10*, 246. https://doi.org/10.3390/aerospace10030246.
37. Hoogreef, M.F.M. Off-Design Performance Consequences of Design Payload and Range Requirements for SPPH Hybrid-Electric Aircraft. In *Proceedings of the CEAS—AIDAA Conference 2025, 12 January 2025*; Materials Research Forum LLC: Millersville, PA, USA, 2026; pp. 607–613.
38. Abu Salem, K.; Palaia, G.; Quarta, A.A. Review of hybrid-electric aircraft technologies and designs: Critical analysis and novel solutions. *Prog. Aerosp. Sci.* **2023**, *141*, 100924. https://doi.org/10.1016/j.paerosci.2023.100924.
39. Quillet, D.; Boulanger, V.; Rancourt, D.; Freer, R.; Bertrand, P. Impact of OEI requirement on parallel hybrid electric turboprop regional aircraft optimization. *AEAT* **2023**, *95*, 276–283. https://doi.org/10.1108/AEAT-02-2022-0051.

40. Moebs, N.; Eisenhut, D.; Windels, E.; van der Pols, J.; Strohmayer, A. Adaptive Initial Sizing Method and Safety Assessment for Hybrid-Electric Regional Aircraft. *Aerospace* **2022**, *9*, 150. https://doi.org/10.3390/aerospace9030150.
41. Botero, E.M.; Wendorff, A.; MacDonald, T.; Variyar, A.; Vegh, J.M.; Lukaczyk, T.W.; Alonso, J.J.; Orra, T.H.; Ilario da Silva, C. SUAVE: An Open-Source Environment for Conceptual Vehicle Design and Optimization. In *Proceedings of the 54th AIAA Aerospace Sciences Meeting 2016, San Diego, CA, USA, 4–8 January 2016*; Curran Associates Inc: Red Hook, NY, USA, 2016; ISBN 978-1-62410-393-3.
42. Lüdemann, M.; Engelmann, M.; Lessis, A.; Türkyilmaz, B.; Maas, P.; Hornung, M. Introduction to the Bauhaus Luftfahrt Aircraft Design Environment (BLADE). *CEAS Aeronaut. J.* 2026, *submitted.*
43. Elmendorp, R.; Vos, R.; La Rocca, G. A conceptual design and analysis method for conventional and unconventional airplanes. In *Proceedings of the 29th Congress of the International Council of the Aeronautical Sciences, St. Petersburg, Russia, 7-12 September2014*; ICAS (The International Council of the Aeronautical Sciences), Ed.; ICAS (The International Council of the Aeronautical Sciences): Bonn, Germany, 2014; ISBN 3932182804.
44. Seitz, A. Rapid Aircraft-Level Evaluation of Revolutionary Propulsion Concepts. In Proceedings of the 13th EASN International Conference, Salerno, Italy, 6 September 2023. https://doi.org/10.5281/zenodo.14800415.
45. Seitz, A.; Donnerhack, S.; Broichhausen, K.; Seifert, J. An Integrated Parametric Model for Engine and Aircraft Design and Performance Optimisation. In *Proceedings of the 44th AIAA/ASME/SAE/ASEE Joint Propulsion Conference & Exhibit, Hartford, CT*; American Institute of Aeronautics and Astronautics: Reston, Virigina, 2008; ISBN 978-1-60086-992-1.
46. Seitz, A.; Maas, P.; Warsch, C.; Böck, R.; Kolb, M.G.; Nittka, J.; Akkaya, M.; Peitsch, D.; Yang, Y.; Möhlenkamp, G.; et al. Multidisciplinary Conceptualisation of Turbo Compressors with Partial Electric Drive. In Proceedings of the 14th EASN International Conference, Thessaloniki, Greece, 11 October 2024.
47. Wegener, E.; Waimer, M.; Schatrow, P. Evaluation of Crashworthy Battery Integration for a Medium-Lift Hybrid-Electric Helicopter Using Full-Scale Simulation. In *Proceedings of the AIAA AVIATION FORUM AND ASCEND 2025, Las Vegas, Nevada*; American Institute of Aeronautics and Astronautics: Reston, Virginia, 2025; ISBN 978-1-62410-738-2.
48. Yang, Y.; Möhlenkamp, G. Sizing and Parameter Study of Compressor Case-Mounted Permanent Magnet Synchronous Motor for Hybrid Electrical Compressor Integration. In *Proceedings of the 73. Deutscher Luft- und Raumfahrtkongress (DLRK), Hamburg, Germany, 30 September–2 October 2024*; DGLR (Deutsche Gesellschaft für Luft- und Raumfahrt), Ed.; Deutsche Gesellschaft für Luft- und Raumfahrt—Lilienthal-Oberth e.V.: Bonn, Germany, 2024.
49. Yang, Y.; Möhlenkamp, G. Analytical model for magnetic field distribution and electromagnetic characteristics analysis of permanent magnet synchronous motor with toroidal winding stator and sinusoidal Halbach array rotor. *IET Conf. Proc.* **2024**, *2024*, 210–217. https://doi.org/10.1049/icp.2024.2159.
50. Schreer, L.; Gümmer, V. Preliminary thermal management system design for cycle-integrated parallel hybrid compressors. *CEAS Aeronaut J* **2026**, *17*, 595–610. https://doi.org/10.1007/s13272-025-00868-5.
51. Nittka, J.; Akkaya, M.; Neumann, N.; Peitsch, D. Aerodynamic pre-design and performance evaluation of counter rotating hybridised compressor concepts: Modelling approach. *CEAS Aeronaut J* **2026**, *17*, 901–911. https://doi.org/10.1007/s13272-025-00894-3.
52. OAG. *Schedules Data 2024*; OAG Aviation Worldwide Limited: Luton, UK, 2024.
53. Federal Aviation Administration (FAA), U.S. Department of Transportation: Fuel requirements for flight in IFR conditions: 14 CFR § 91.167. Code of Federal Regulations; U.S. Government Publishing Office: Washington, DC, USA, 2000.
54. Leishman, J.G. *Principles of Helicopter Aerodynamics*, 2rd ed.; Cambridge University Press: Cambridge, UK, 2006; ISBN 978-0-521-85860-1.
55. Vratny, P. Conceptual Design Methods of Electric Power Architectures for Hybrid Energy Aircraft. Ph.D. Thesis, TUM (Technische Universität München), Munich, Germany, 2018.
56. Obert, E. *Aerodynamic Design of Transport Aircraft;* IOS Press: Amsterdam, Netherlands, 2009; ISBN 9781586039707.
57. Layton, D.M. *Introduction to Helicopter Conceptual Design*; American Institute of Aeronautics and Astronautics (AIAA) Professional Studies Series: Salinas, CA, USA, 1992.
58. Hajek, M. *Auslegung und Entwurf von Hubschraubern 1: Lecture Notes*; Lehrstuhl für Hubschraubertechnologie, Technical University of Munich, Munich, Germany, 2018.
59. Taylor, J.W.R. *Jane's all the World's Aircraft,1980-81/Ompiled and Edited by John W.R. Taylor*; Janes Publishing Company Limited: London, UK, 1980; ISBN 0710607059.
60. Knöös Franzén, L.; Staack, I.; Krus, P.; Amadori, K. Optimization Framework for Early Conceptual Design of Helicopters. *Aerospace* **2022**, *9*, 598. https://doi.org/10.3390/aerospace9100598.

61. Raymer, D.P. *Aircraft Design: A Conceptual Approach*, 4th ed.; American Institute of Aeronautics and Astronautics: Reston, VA, USA, 2006; ISBN 978-1-56347-829-1.
62. Pratt, J.; Klebanoff, L.; Munoz-Ramos, K.; Akhil, A.; Curgus, D.; Schenkman, B. *Proton Exchange Membrane Fuel Cells for Electrical Power Generation On-Board Commercial Airplanes*; Sandia National Laboratories: Albuquerque, NM, USA, 2011.
63. Prouty, R.W. *Helicopter Performance, Stability, and Control;* PWS Engineering: Boston, MA, USA, 1986; ISBN 978-0534063603.
64. Johnson, W. *Helicopter Theory*, Unabridged and slightly corr. republ; Dover Publ: New York, NY, USA, 1994; ISBN 978-0486682303.
65. Kaiser, S.; Seitz, A.; Donnerhack, S.; Lundbladh, A. Composite Cycle Engine Concept with Hectopressure Ratio. *J. Propuls. Power* **2016**, *32*, 1413–1421. https://doi.org/10.2514/1.B35976.
66. Kaiser, S.; Kellermann, H.; Nickl, M.; Seitz, A. A Composite Cycle Engine Concept for Year 2050. In *Proceedings of the 31st Congress of the International Council of the Aeronautical Sciences, Belo Horizonte, Brazil, 9–14 September 2018*; ICAS (The International Council of the Aeronautical Sciences), Ed.; The International Council of the Aeronautical Sciences: Bonn, Germany, 2018; ISBN 9783932182884.
67. Kurzke, J. GasTurb 12—Design and Off-Design Performance of Gas Turbines, Germany, 2013. Available online: http://www.gasturb.de/Gtb12Manual/GasTurb12.pdf (accessed on 2 March 2019).
68. Kurzke, J. *Compressor and Turbine Maps for Gas Turbine Performance Computer Programs—Issue 3*, GasTurb GmbH: Aachen, Germany, 2013.
69. McBride, B.J.; Gordon, S. Computer Program for Calculation of Complex Chemical Equilibrium Compositions and Applications. Part 2: Users Manual and Program Description NASA-RP-1311; E-8017-1, 1996. Available online: https://ntrs.nasa.gov/citations/19960044559 (accessed on 1 October 2026).
70. Seitz, A. Advanced Methods for Propulsion System Integration in Aircraft Conceptual Design. Ph.D. Thesis, TUM (Technische Universität München), Munich, Germany, 2012.
71. Grieb, H. *Projektierung von Turboflugtriebwerken;* Birkhäuser Verlag: Basel, Switzerland, 2004; ISBN 978-3-0348-7938-5.
72. A. Alexiou; I. Roumeliotis; N. Aretakis; A. Tsalavoutas; K. Mathioudakis. Modeling Contra-Rotating Turbomachinery Components for Engine Performance Simulations: The Geared Turbofan With Contra-Rotating Core Case. *J. Eng. Gas Turbines Power* **2012**, *134*, 111701. https://doi.org/10.1115/1.4007197.
73. Rick, H. *Gasturbinen und Flugantriebe*: *Grundlagen, Betriebsverhalten und Simulation;* Springer Berlin Heidelberg: Berlin, Heidelberg, 2013; ISBN 978-3-540-79446-2.
74. Yang, Y.; Henke, M.; Möhlenkamp, G. Analytical Investigation of Short-Circuit Protection and Post-Fault Operation in Dual Three-Phase PMSMs for Hybrid Electric Counter-Rotating Compressor Applications. *IEEE Access* **2026**, *14*, 17303–17323. https://doi.org/10.1109/ACCESS.2026.3658195.
75. Seitz, A.; Habermann, A.L.; van Sluis, M. Optimality considerations for propulsive fuselage power savings. *Proc. Inst. Mech. Eng. Part G J. Aerosp. Eng.* **2021**, *235*, 22–39. https://doi.org/10.1177/0954410020916319.
76. Chati, Y.; Balakrishnan, H. Analysis of Aircraft Fuel Burn and Emissions in the Landing and Take Off Cycle using Operational Data. In Prooceedings of the 6th International Conference on Research in Air Transportation (ICRAT 2014), Istanbul, Turkey, 26–30 May 2014.
77. Airbus S.A.S. Customer Service. *A320 Aircraft Characteristics Airport and Maintenance Planning*; Airbus S.A.S.: Toulouse, France, 2017.
78. Goulos, I.; Ali, F.; Tzanidakis, K.; Pachidis, V.; D'Ippolito, R. A Multidisciplinary Approach for the Comprehensive Assessment of Integrated Rotorcraft–Powerplant Systems at Mission Level. *J. Eng. Gas Turbines Power* **2015**, *137*, 012603. https://doi.org/10.1115/1.4028181.
79. Leonardo S.p.A. *AW189K—Program Management Review*; Leonardo S.p.A.: Bordes, France, 2021.
80. Bristow Group Inc. Heavy Twins—Leonardo AW189. Available online: https://www.bristowgroup.com/fleet/heavy-twins/leonardo-aw189 (accessed on 16 August 2026).
81. International Civil Aviation Organization. *Annex 14 to the Convention on International Civil Aviation*: *Aerodromes, Volume I: Aerodrome Design and Operations*, 9th ed.; Annex 14; ICAO: Montreal, Canada, 2022; Volume I. Available online: https://elibrary.icao.int/product/274803 (accessed on 16 August 2026).
82. UK Civil Aviation Authority. *Standards for Offshore Helicopter Landing Areas*, 9th ed.; Amendment 1; CAP 437; UK Civil Aviation Authority: London, UK, 2026. Available online: https://www.caa.co.uk/data-and-publications/publications/documents/content/cap-437/ (accessed on 16 August 2026).

83. Hoogreef, M.; Zuijderwijk, N.; Scheers, E.; Proesmans, P.-J.; Santos, B.F. Coupled Hybrid & Electric Aircraft Design and Strategic Airline Planning. In *Proceedings of the AIAA AVIATION 2023 Forum, San Diego, CA, USA and Online*; AIAA (The American Institute of Aeronautics and Astronautics), Ed.; American Institute of Aeronautics and Astronautics: Reston, Virginia, 2023; ISBN 978-1-62410-704-7.
84. Rischmüller, U.C.J.; Lessis, A.; Egerer, P.; Hornung, M. Conceptual Design of a Hydrogen-Hybrid Dual-Fuel Regional Aircraft Retrofit. *Aerospace* **2024**, *11*, 123. https://doi.org/10.3390/aerospace11020123.
85. Seitz, A.; Maas, P.; Böck, R.; Kolb, M.G.; Peitsch, D.; Schreer, L.; Gümmer, V.; Yang, Y.; Möhlenkamp, G. Multidisciplinary Conceptual Design of Turbo Compressors with Partial Electric Drive. *Aerosp. J.* 2026, *submitted.*
86. Atanasov, G.; Silberhorn, D. Hybrid Aircraft for Improved Off-Design Performance and Reduced Emissions. In *Proceedings of the AIAA SCITECH 2020 Forum, Orlando, FL, USA, 6–10 January*; American Institute of Aeronautics and Astronautics (AIAA): Reston, VA, USA, 2020; ISBN 978-1-62410-595-1.

Disclaimer/Publisher's Note: The statements, opinions and data contained in all publications are solely those of the individual author(s) and contributor(s) and not of MDPI and/or the editor(s). MDPI and/or the editor(s) disclaim responsibility for any injury to people or property resulting from any ideas, methods, instructions or products referred to in the content.